

Dynamic Shake-Table Testing and Analytical Investigation of Self-Centering Steel Plate Shear Walls

Daniel M. Dowden, P.E., S.E.¹; and Michel Bruneau, F.ASCE²

Abstract: Recent research has shown that self-centering steel plate shear walls (SC-SPSWs) offer an enhanced seismic performance over conventional steel plate shear walls by providing an additional self-centering capability using steel frames detailed with posttensioned (PT) beam-to-column rocking connections. As with other previously proposed self-centering frames detailed with similar beam-to-column connections, this detailing facilitates the incorporation of replaceable energy dissipation components, as part of the lateral force resisting system (LFRS). In doing so, by design, the gravity frame components of the LFRS are also protected from damage during an earthquake. To investigate the dynamic seismic response of this proposed structural system, one-third scaled SC-SPSW specimens were subjected to ground motions during a series of dynamic shake-table tests. The experimental investigation results presented in this paper are the first shake-table tests conducted on SC-SPSWs. This test program was composed of two three-story single-bay SC-SPSW frames, each with a different PT beam-to-column connection. For one frame type, connections rock about both beam flanges; for the other, connections rock about the top beam flanges only (referred to as the NewZ-BREAKSS connection). The latter connection essentially eliminates PT boundary frame expansion (a.k.a., beam-growth) that occurs with connections that rock about both beam flanges. Furthermore, both an infill web plate and a bidirectional infill web strip layout were investigated as alternative infill configurations. Results show that the presence of infill web plate compression strength has no significant effect on recentering of the frame (contrary to what has been reported in the literature for quasi-static tests). Furthermore, presented analytical expressions that describe the drift induced infill web plate strains and posttension demands for beam-to-column rocking joints are found to compare well with the experimental results, but conservatively overestimate the PT demands. Numerical models were able to reasonably estimate the peak roof drift and maximum base shear demands. This paper presents information on the actual seismic response of SC-SPSWs detailed with a flange-rocking and the NewZ-BREAKSS posttensioned rocking joint connections, along with analytical equations that could be used to inform some aspects of design. DOI: 10.1061/(ASCE)ST.1943-541X.0001547. © 2016 American Society of Civil Engineers.

Author keywords: Self-centering; Steel plate shear wall; Moment frame; Rocking connection; Seismic response; Resilient structure; Seismic performance; Shake-table testing; Seismic effects.

Introduction

Recent research has shown that a self-centering steel plate shear wall (SC-SPSW) is a robust, ductile, and easily repaired system, making these systems attractive for use in buildings located in areas of high seismicity (Winkley 2011; Clayton 2013; Dowden 2014). Similar to other previously proposed self-centering steel frame systems (e.g., Ricles et al. 2002; Christopoulos et al. 2002; Garlock et al. 2005; Rojas et al. 2005), the main performance objectives of this lateral force resisting system (LFRS) are to: (1) provide building recentering through the use of posttensioned (PT) beam-to-column rocking connections, and (2) protect the gravity frame components of the LFRS by concentrating inelastic energy dissipation to replaceable elements. Accordingly, the PT boundary frame is designed to remain essentially elastic, where the decoupling of the PT boundary frame from the energy dissipation components of the

LFRS, is achieved through the use of PT beam-to-column rocking connections, in lieu of conventional rigid moment connections.

To better understand the dynamic response of any newly proposed LFRS, dynamic shake-table testing is necessary to confirm that the system have satisfactory performance subjected to actual simulated dynamic earthquake loadings. Experimental shake-table testing has previously been conducted by researchers on other self-centering steel frame systems (e.g., Wang 2007; Pollino and Bruneau 2008; Ma et al. 2011; Erochko et al. 2013; Wiebe et al. 2013), but investigation through shake-table testing is still limited for self-centering frame systems. This paper presents results on the first proof-of-concept of the SC-SPSW through shake-table testing.

The results presented in this paper were part of a two-phase experimental program consisting of quasi-static cyclic testing followed by dynamic shake-table testing. The quasi-static cyclic tests provided significant information on the inelastic behavior of SC-SPSWs, in terms of energy dissipation, ductility, self-centering response, and other response factors; information and results from those tests are presented elsewhere (Dowden and Bruneau 2014). The focus in this paper is on results from the shake-table test program, which consisted of six shake-table tests of one-third scaled, single-bay, three-story SC-SPSW frames. Furthermore, two frame types were investigated, each with a different beam-to-column posttensioned (PT) rocking joint. The first joint detail consisted of a top and bottom beam flange-rocking (FR) connection detail previously investigated by other researchers in steel moment frames (see earlier references). The second joint detail consisted of a beam-to-column joint that rocks about the top beam flange only and is

¹Research Engineer, Structural Engineering and Earthquake Simulation Laboratory, Dept. of Civil, Structural, and Environmental Engineering, Univ. at Buffalo, Buffalo, NY 14260 (corresponding author). E-mail: dmdowden@buffalo.edu

²Professor, Dept. of Civil, Structural, and Environmental Engineering, Univ. at Buffalo, Buffalo, NY 14260.

Note. This manuscript was submitted on February 14, 2015; approved on February 23, 2016; published online on May 9, 2016. Discussion period open until October 9, 2016; separate discussions must be submitted for individual papers. This paper is part of the *Journal of Structural Engineering*, © ASCE, ISSN 0733-9445.

referred to as the NewZ-BREAKSS (NZ) connection. This latter connection was proposed by Dowden and Bruneau (2011), inspired by connections proposed by others (e.g., Clifton et al. 2007; MacRae et al. 2009; Mander et al. 2009; Khoo et al. 2011), to eliminate the PT boundary frame expansion (a.k.a., beam-growth) that occurs with the FR connection. In addition, for each frame type (i.e., FR and NZ), three different configurations were investigated, namely specimens having solid infill web plates (W), infill web strips (S), and no infill web plates/strips (B).

In this paper, the prototype building and scaling procedure used for the shake-table tests are first presented, providing some background on the anticipated specimen response. Next, details of the specimens are presented along with the test setup and shake-table loading protocol. The experimental results are then presented for the global response in terms of base shear versus roof drift, self-centering response in terms of residual roof drifts, and PT beam-to-column rocking joint response in terms of beam PT response history. Next, the numerical models developed using the program *OpenSees* (Mazzoni et al. 2009) are presented, followed by comparison of numerical results with the experimental results. For this purpose, incremental dynamic pushover curves (in terms of maximum absolute base shear and peak roof drift demands) were generated based on nonlinear dynamic response history analyses and compared to the experimental ones. Additionally, analytical expressions are presented for the drift induced PT force response. Results using these equations, in addition to numerical results obtained from *OpenSees* analyses, are then compared to those obtained experimentally.

An important detailing consideration for SC-SPSWs is the corner detail of the infill web plates, which is subjected to large tensile strains due to the added effect of the gap opening at the beam-to-column rocking joints. If not properly detailed, a premature unzipping effect of the infill web plate tearing from the boundary frame could occur, initiating from the infill web plate corners. To mitigate this, a corner cut-out detail of the web plates is critical to delay such effects. For this purpose, an analytical relationship describing the kinematics of the idealized tension-field of the infill web plate was established and the predicted response is compared with the experimental.

Prototype Building and Scaling

The boundary frame specimens used in the dynamic shake-table tests were used previously by Dowden and Bruneau (2014) to experimentally investigate the quasi-static cyclic behavior of SC-SPSWs (as these boundary frames were designed to remain essentially elastic). For the quasi-static tests, the specimens were designed based on the parameters of the three-story building used in the SAC Steel Project (FEMA 2000). This prototype building is representative of a standard office building with structural steel frame construction and assumes a total of six lateral force resisting frames in each primary building direction. The building site location was assumed to be in Los Angeles, California situated on stiff soil (Site Class D per ASCE 7-10 definition). The earthquake spectral response acceleration parameters used were based on the 2009 NEHRP seismic hazard maps, with a 5% viscous damping design spectral response acceleration at short (S_{DS}) and 1 s (S_{D1}) periods of 1.598 g and 0.842 g, respectively. The corresponding Design Response Spectrum (DRS) is shown in Fig. 1 (also shown is the ground motion spectrum, which will be addressed subsequently with the loading protocol).

The preliminary design for the single-bay three-story prototype frame assumed a conventional steel plate shear wall frame using established design procedures per AISC (2005). The equivalent lateral force procedure per ASCE 7-10 (ASCE 2010) was performed

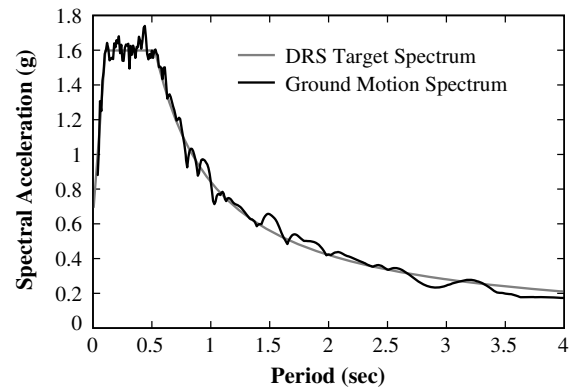


Fig. 1. Ground motion response spectrum

to obtain design seismic forces for the prototype frame using the following parameters: R = response modification factor = 7; I = importance factor = 1. The total seismic building weight was assumed to be equally distributed among the six frames in each primary direction for a tributary seismic weight of 1,084 kips per frame. For final specimen design, a numerical model of the scaled specimen (presented later in this paper), based on a scale factor of three (i.e., one-third scale of the prototype in order to facilitate testing), was developed for the SC-SPSW where nonlinear pushover analyses using a strip model (Sabelli and Bruneau 2007) was performed.

For the shake-table tests, the specimen parameters (i.e., member sizes and infill web plate thicknesses) and design criteria (i.e., DRS parameters) were identical to the previously conducted quasi-static tests. However, because of operating constraints of the shake-table capacity, to be able to subject the specimen to large inelastic deformations, it could not be related to the original prototype building. Although the specimen did not need to be related to a prototype building for the testing program to give meaningful results, to establish such a linkage, the prototype building footprint was reduced, leading to a tributary seismic weight for each of the six prototype lateral frames of 2,042 kN (459 kips) per frame. The shake-table prototype building is presented in Fig. 2. Additional information on scaling as it relates to the shake-table and quasi-static prototype buildings can be found in Dowden and Bruneau (2014).

Modifying the prototype building parameters (from the original prototype building for which the specimen design was originally based) has an effect on the interpretation of the seismic performance and response of the test specimens. To investigate the implications of this on the expected specimen response, using frame

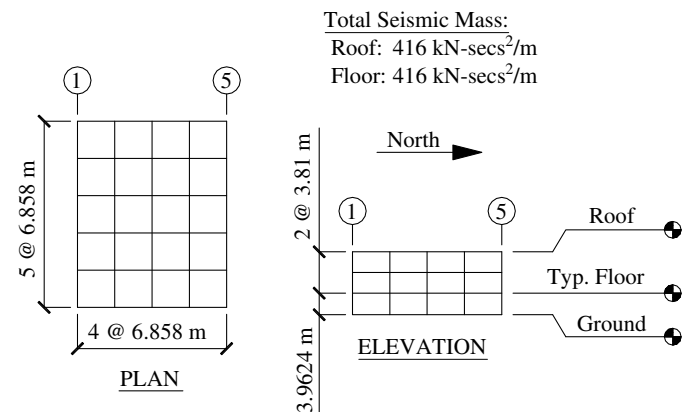


Fig. 2. Prototype building

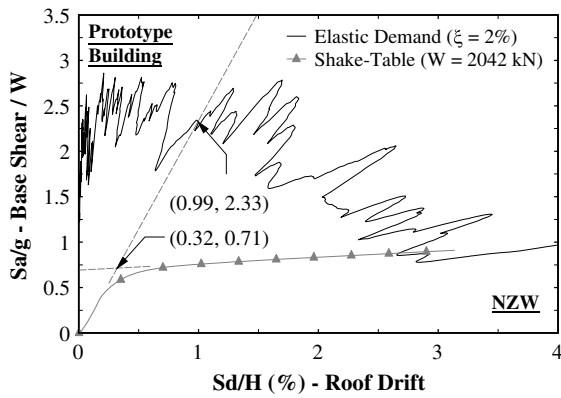


Fig. 3. Prototype frame spectral response

NZW to illustrate, a spectral analysis was performed to obtain the approximate response modification factor, R , of the shake-table prototype frame. As part of the spectral analysis, a nonlinear pushover analysis of the prototype SC-SPSW is required in order to obtain the spectral demand curve. Although the numerical modeling of SC-SPSWs is presented later in this paper, the results of the pushover analysis are presented here. As shown in Fig. 3, the approximate R factor was calculated to be 3.3, which is approximately 50% of that assumed in the original design noted earlier (i.e., $R = 7$). As a result of this difference, the seismic responses of the shake-table specimens are expected to exhibit less inelastic drifts than would have been the case if the prototype building parameters of the original prototype building could have been implemented for the shake-table tests (i.e., if the capacity of the shake-table was not an issue).

Although it is convenient to associate the shake-table tests to a full-scale prototype building to provide some level of reference, the primary objective of these tests was not to establish the ultimate behavior of the SC-SPSWs (which was accomplished by the quasi-static tests), but rather to observe the behavior of SC-SPSWs subjected to dynamic earthquake simulation loadings. The loading

protocol is presented in the subsequent section, but it is relevant in this instance that it follows an incremental dynamic pushover format. In particular, shake-table testing of the specimens continued up to the safe operating limits of the shake-table and/or specimens. Thus, the definition of a prototype building as it pertains to these tests is not necessarily critical because of the manner in which the tests were conducted.

Test Specimens, Setup, and Loading Protocol

A schematic of a test specimen is shown in Fig. 4 for frame FR (frame NZ similar), along with two different beam-to-column joint details. In that figure, the beams and columns are referred to as HBE (horizontal boundary element) and VBE (vertical boundary element) members, respectively, in keeping with accepted nomenclature for SPSWs (AISC 2005, 2010). Furthermore, as noted in the "Introduction," in addition to an infill web plate configuration, an infill web strip configuration was investigated. The infill web strips were oriented in right-leaning and left-leaning configurations and installed on the opposite sides of the HBE and VBE fish plates. The typical layout of the infill web strips for one side of the frame is presented in Fig. 5. The spacing and width of the strips was controlled by the selection of clear distance between strips to avoid any physical interaction of the strips during testing. For the specimens, a clear distance of approximately 3.5 in. was selected. Additionally, as observed in the figure, there are two different strips widths. The 3 in. strips are the typical strips and the 4.5 in. strips are provided near the HBE-to-VBE joints and are wider to take into consideration that a strip cannot be provided in-line with the rocking joints. In other words, the widths of the infill strips near the HBE-to-VBE joints were increased because of the increased clear spacing of those locations based on tributary area. This infill web strip configuration was originally conceived as a way to investigate SC-SPSW response while having a better knowledge of the demands from tension-field action because when using infill web strips the angle-of-inclination of the tension-field can be precisely known. For the specimens in this testing program, thickness of the strips at each level matched that of the infill web plate configuration.

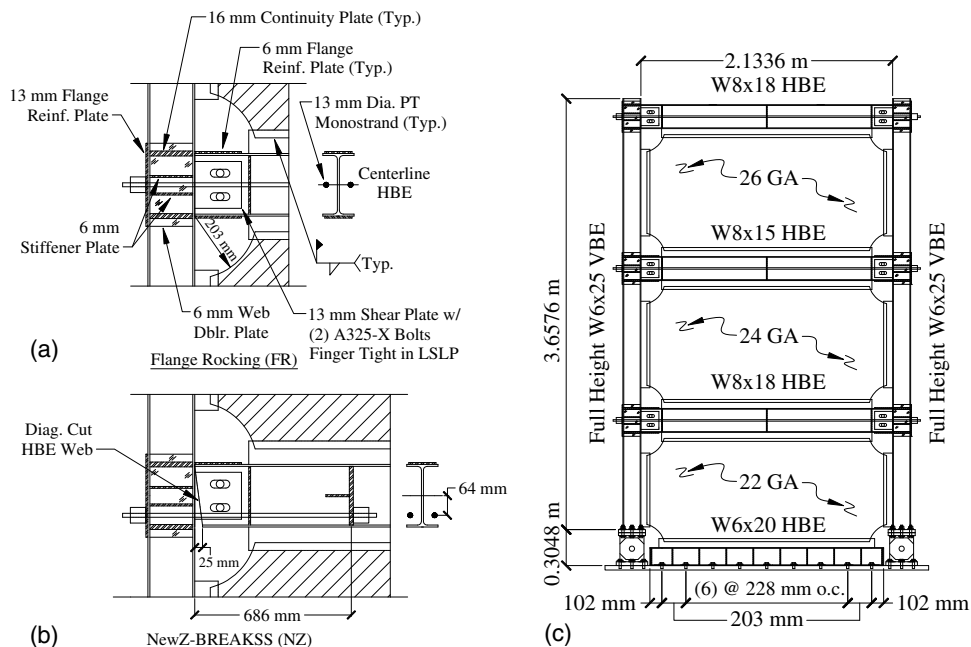


Fig. 4. Specimen: (a) FR conn; (b) NZ conn; (c) frame FR elevation (NZ similar)

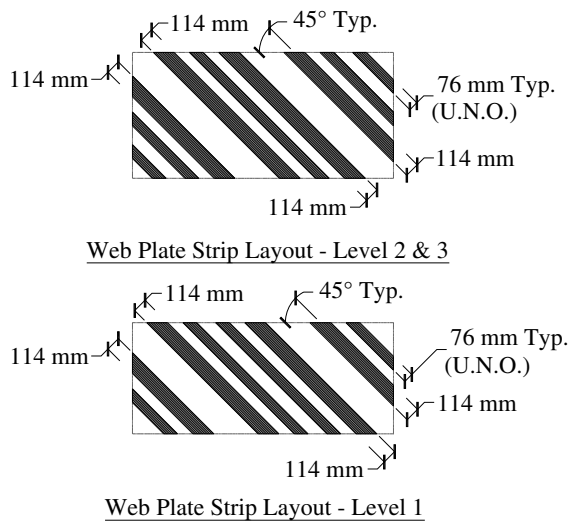


Fig. 5. Infill web strip layout

The distribution of infill web strips presented in Fig. 5, resulted in an approximate 50% reduction in total infill web plate area (i.e., compared to a solid infill web plate configuration). The consequence of this is that the strength of the frames with infill web strips is approximately 50% of that for the frames with the infill web plates (i.e., proportional to the area of infill not covered by the strips).

Furthermore, as shown in Fig. 4(c), at the foundation level a clevis and pin connection was provided at the VBE base to allow free rotation without the formation of a plastic hinge. Additionally, an anchor beam bolted to the foundation anchor plate was provided for connection of the infill web plates. An initial posttensioning force, P_o , of approximately 40–45% of the PT yield strength for each monostrand was targeted for both the FR and NZ frames, where the PT yield strength, $F_{y,PT}$, was assumed to be 90% of the ultimate tensile strength, F_{uPT} , of the PT strands. Note that the value of initial posttensioning force should be provided to ensure that the PT elements remain elastic at a select target design drift. Therefore, in part, the initial PT force is dependent on the building drift performance objective selected by the design engineer. Specifically, the axial tension forces in the PT elements include

the initial PT force plus an incremental PT force attributable to PT elongations during frame drift. For frame recentering, it would be desired to provide the largest initial PT force for a given target design drift. For the specimens in the shake-table testing reported here, a 4% drift was selected as a target upper limit for an elastic PT design, which facilitated the selection of the target initial PT forces.

Each PT boundary frame type was constructed only once. This means that through each frame test sequence (i.e., the same frame was retested with different types of infill, as explained later), no alterations were made to the PT elements from the initial frame construction. As such, PT losses are cumulative and carried over to each subsequent test of each sequence. This had some influence on the PT force responses (to be presented subsequently). Instrumentation was provided to record local and global responses and included displacement transducers, load cells, accelerometers, krypton sensors, and strain gages. Additional information on the test setup and instrumentation is provided in Dowden and Bruneau (2014).

The test setup on the shake-table and a schematic of the test setup are shown in Figs. 6 and 7, respectively. As shown, the test specimen is located between two sets of lateral bracing systems. This system is referred to as the gravity mass frame (GMF) and was previously designed at the University at Buffalo (Kusumastuti 2005). The GMF system is designed to be a self-contained structure that can support its own gravity weight, has lateral stiffness and stability in its primary transverse direction, but has essentially no lateral stiffness in its longitudinal direction (facilitated by semi-spherical rocker plates at the top and bottom of the GMF columns, of which a photograph is presented in Fig. 7). Each set of gravity columns supports a 89 mm (3.5 in.) thick steel plate weighing approximately 38 kN (8.5 kips) each, providing an approximate seismic weight of 76 kN (17 kips) per level, for a total of 227 kN (51 kips). Inertia forces are transferred from the GMF mass plates to the specimen at the diaphragm connections at the ends and at mid-span of each HBE, as shown in Fig. 7. The test setup is an approximate idealization of the prototype frame in a building. In particular, the interaction effects with the surrounding gravity frame that would be present in an actual building are not present. However, the primary objective of these shake-table tests is to investigate the fundamental dynamic system response of the SC-SPSW, and rigorous correlation with the prototype was not necessary for this purpose.

Typically a suite of GMs would be used for design to take into consideration the variability of individual GM characteristics, with

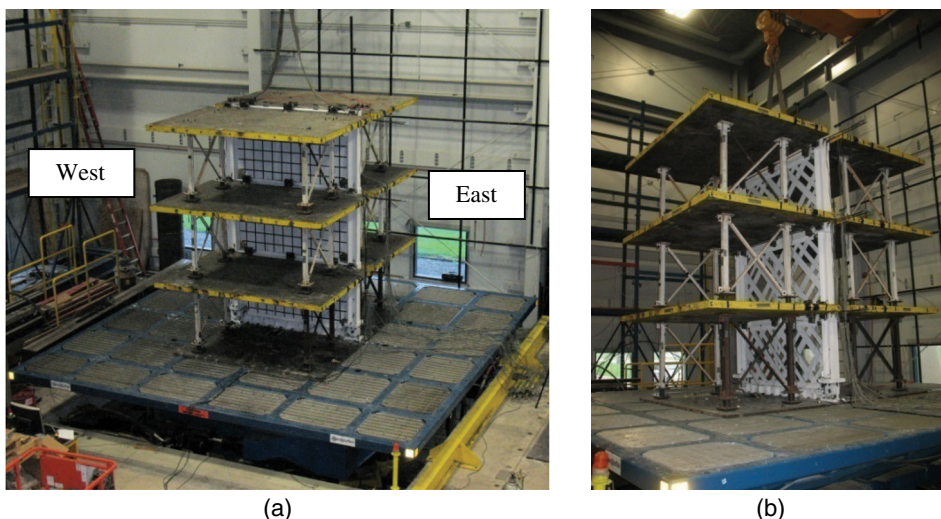


Fig. 6. Test setup: (a) infill web plate; (b) infill web strips

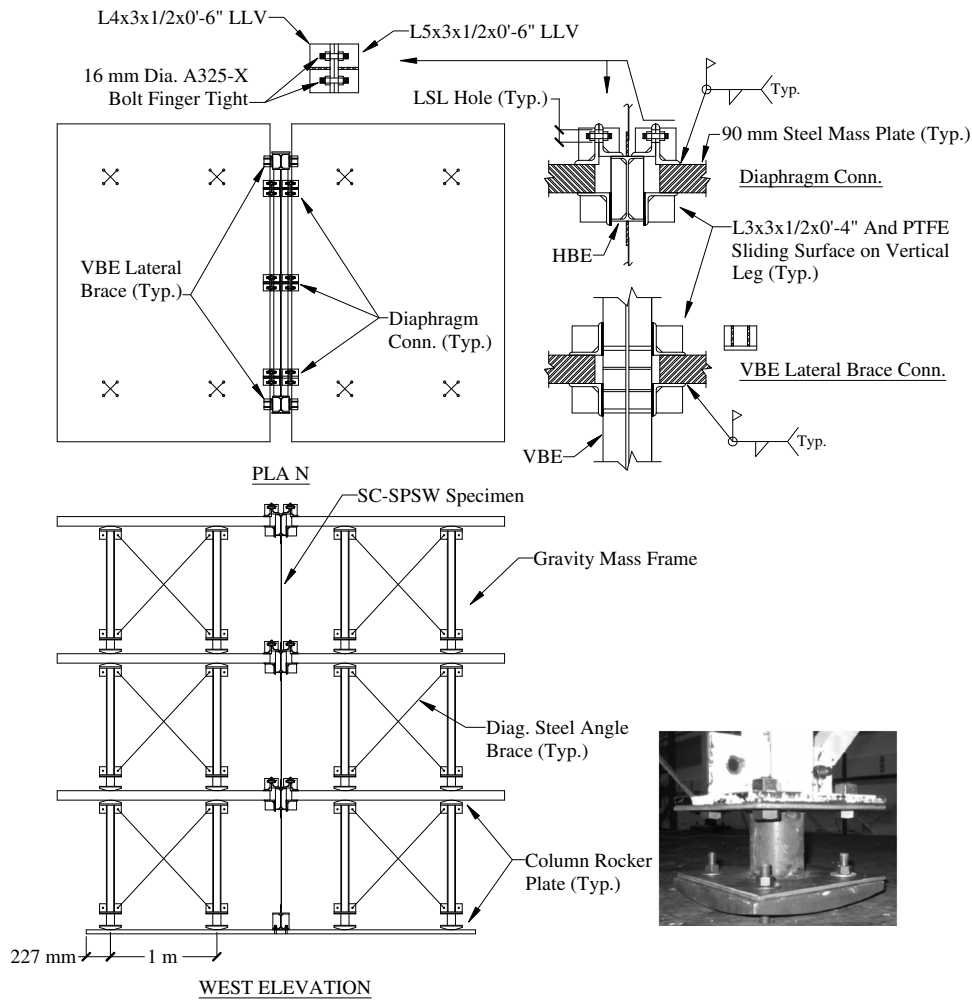


Fig. 7. Test setup details

the objective of obtaining a median and/or average response matching the DRS. For the shake-table tests conducted here, this was not practical. Therefore, the loading protocol consisted of amplitude scaling a single synthetic GM, beginning with low level amplitude intensities, and for subsequent ground motions with increased scaled amplitudes. For this purpose, a spectrum-compatible synthetic GM (matching the DRS) was generated using the target acceleration spectra compatible time histories (TARSCTHS) code, by Papageorgiou et al. (1999). The corresponding DRS and GM spectrum are shown in Fig. 1 and are comparable. For the shake-table tests, the synthetic GM was time compressed based on similitude law for the scaled specimens. Additionally, for the frames with infill web plates/strips, the tests concluded with the GM scaled to levels ranging between 25 and 50% of DRS (arbitrarily assuming aftershocks of these intensities) to investigate frame response after the infill web plates/strips have yielded significantly. Furthermore, to establish natural frequencies of the specimens and quantify changes in dynamic properties, white noise (i.e., an acceleration-controlled flat-spectrum broadband random motion) identification tests were conducted prior to each GM amplitude test and at the conclusion of each test series.

The loading sequence for each test is summarized in Tables 1 and 2 for frames FR and NZ, respectively. The nomenclature used to differentiate each test specimen follow, where the acronym is appended to the frame type (i.e., FR or NZ): W = full infill web plate, B = no infill web plate/strips, and S = infill web strips.

For example, FRW = flange-rocking frame with infill web plate; NZB = NewZ-BREAKSS frame with no infill web plate/strips; and so on. The tests were performed sequentially as follows: FRW, FRB, FRS, NZW, NZB, and NZS. Additionally, for the experimental results presented subsequently, a positive drift corresponds to an eastward drift direction. Note that the differences in GM loadings between each test setup (i.e., FRW, FRS, etc.) were attributable to the adjustment of the loading sequence on a case-by-case basis during testing, to ensure not overtesting the specimen (i.e., to collapse) and to ensure testing within the safe operating limits of the shake-table. As an example, rocking resonance occurred with test frames FRB and FRS (which will be presented later), which then affected the loading protocol used for test frames NZB and NZS.

Experimental Results

For the loading protocol presented above, the GM target PGA for frames FR and NZ are shown in Tables 1 and 2, respectively. The comparison of the target and achieved acceleration responses shown in Figs. 8(a and b) for frames FR and NZ, respectively, for the 100% GM, is representative of the fidelity achieved in all tests. The comparison is provided in terms of acceleration response spectra. For this purpose, 5% damping is used, because this is the original criterion (and input parameter) that was used to generate the synthetic GM. The achieved acceleration response is taken

Table 1. Frame FR Loading Sequence

GM amplitude	PGA	
	%GM	g
	Test frame FRW	
WN	—	0.15
1	10	0.07
2	25	0.18
WN	—	0.15
3	50	0.36
WN	—	0.15
4	75	0.53
WN	—	0.15
5	100	0.71
WN	—	0.15
6	120	0.85
WN	—	0.15
7	140	1.00
WN	—	0.15
8	50	0.36
WN	—	0.15
	Test frame FRB	
WN	—	0.10
1	10	0.07
2	25	0.18
WN	—	0.10
	Test frame FRS	
WN	—	0.05
1	10	0.07
WN	—	0.05
2	25	0.18
WN	—	0.05
3	50	0.36
WN	—	0.05
4	75	0.53
WN	—	0.05
5	100	0.71
WN	—	0.05
6	25	0.18
WN	—	0.05

Note: WN = white noise excitation.

from the accelerometer sensors located at the northeast and south-east corners of the shake-table, corresponding to the acceleration in the longitudinal frame direction (i.e., east-west). Furthermore, the initial elastic fundamental period obtained from the corresponding transfer functions (i.e., Fourier transform of a story level acceleration time history normalized by the Fourier transform of the base acceleration time history) of the white noise identification tests (Fig. 9) is superimposed for reference. In general, it is observed that the target and achieved spectra compare reasonably well in the anticipated period range of the test specimens (i.e., in the range of periods larger than the initial fundamental period shown). Shake-table measured displacements and accelerations (not shown here) were also verified to accurately match their respective command signals.

Base Shear versus Roof Drift

The global response in terms of base shear versus roof drift is presented in this section, where the base shear was obtained as the summation of the total acceleration response measured from accelerometers at each story level, multiplied by the approximate mass at each corresponding level. Furthermore, the raw acceleration data

Table 2. Frame NZ Loading Sequence

GM amplitude	PGA	
	%GM	g
	Test frame NZW	
WN	—	0.10
1	10	0.07
WN	—	0.10
2	25	0.18
WN	—	0.10
3	50	0.36
WN	—	0.10
4	75	0.53
WN	—	0.10
5	100	0.71
WN	—	0.10
6	120	0.85
WN	—	0.10
7	140	1.00
WN	—	0.10
8	140	1.00
WN	—	0.10
9	50	0.36
WN	—	0.10
	Test frame NZB	
WN	—	0.10
1	10	0.07
2	15	0.11
3	20	0.14
4	25	0.18
5	30	0.21
6	35	0.25
7	40	0.29
8	45	0.23
9	50	0.36
WN	—	0.10
	Test frame NZS	
WN	—	0.05
1	5	0.04
WN	—	0.05
2	13	0.09
WN	—	0.05
3	25	0.18
WN	—	0.05
4	38	0.27
WN	—	0.05
5	50	0.36
WN	—	0.05
6	60	0.43
WN	—	0.05
7	70	0.50
WN	—	0.05
8	90	0.64
WN	—	0.05
9	100	0.71
WN	—	0.05
10	38	0.27
WN	—	0.05

Note: WN = white noise excitation.

was modified using a low-pass filter with a cut off frequency of 20 Hz. The acceleration data was filtered due to the presence of undesired high frequency content observed using the raw accelerometer data. In part, this was attributed to the effects of the HBE-to-VBE gap opening and closing (which generates an impact force at the HBE-to-VBE flanges); this effect was more prominent in frame

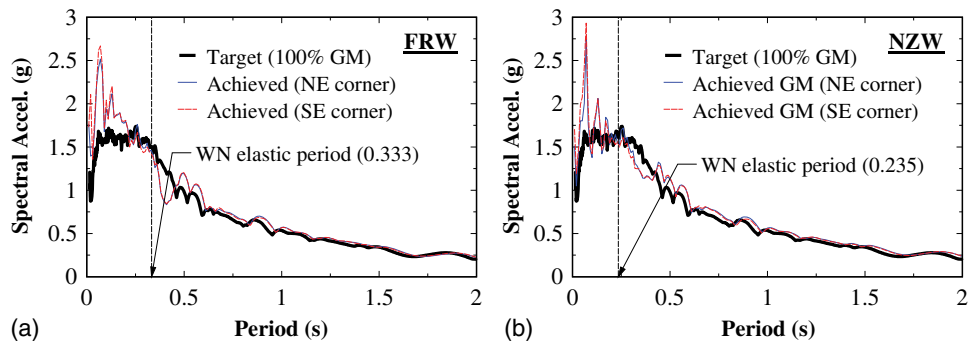


Fig. 8. Achieved versus target shake-table input ground motion: (a) FRW; (b) NZW

FR (i.e., such effects are not as pronounced for frame NZ because an initial gap is provided at the HBE bottom flanges and the HBE top flanges remain in contact with the VBEs). The cut off frequency was chosen to ensure that as a minimum, the first two modes were present. This was based on a modal analysis performed on the numerical model, indicating that the cumulative modal participating mass ratio through the second mode was approximately 95%. This was also confirmed from the white-noise transfer functions presented in Fig. 9, which show that the effects of the third and higher modes are insignificant.

Furthermore, the base excitation for the shake-table tests was in the primary longitudinal direction (i.e., east-west) of the test specimen. In that direction, some rotation of the test specimen developed because of rocking effects of the shake-table, as it resisted the base reactions of the test specimen. Measured peak rotations of the shake-table ranged between 0.05 to 0.15 degrees. As a consequence, the total linear displacements recorded by the string potentiometers used to measure story displacements, also include a horizontal component attributable to shake-table rotation. Accordingly, the additional horizontal displacement due to the effects of the shake-table rotation (from rigid-body rotation, Δ = shake-table rotation in units of radians \times height) was subtracted from the string potentiometer raw data.

The concatenation of all GM amplitude test results of the global base shear normalized by the total effective seismic weight (i.e., $W = 227$ kN, or 51 kips) versus roof drift response along with

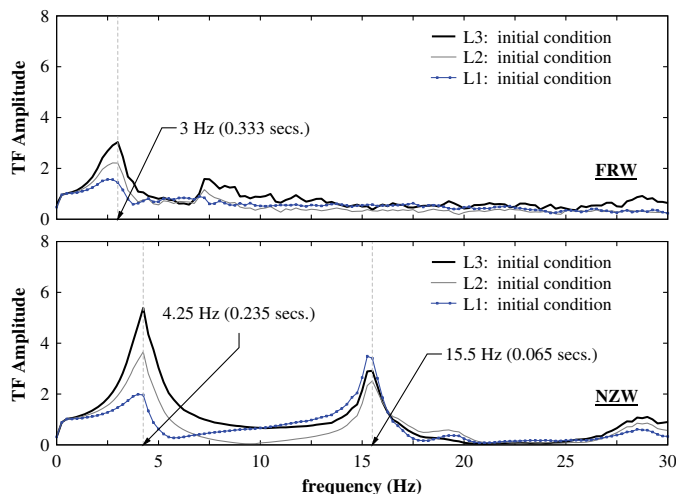


Fig. 9. White noise transfer function

the end-of-test residual drifts at each GM amplitude test is shown in Figs. 10 and 11 for frames FR and NZ, respectively. Furthermore, in these figures, for frames with infill web plates/strips, the global force-displacement response for the PT boundary frame is superimposed for reference (for reasons presented subsequently). A maximum value of 0.2% residual roof drift was used as the criterion for frame recentering, corresponding to the code-acceptable out-of-plumb tolerances for new construction. For convenience, this threshold is indicated by the horizontal dashed lines provided in the residual roof drift results. From the global base shear versus roof drift results presented, the following observations are supported:

- For frames FRW and NZW, the fatness in the hysteresis curve near the zero-drift location is partly attributed to compression strength of the infill web plate created by the way the infill web plate plastically deforms when tension-field action develops during frame drift. Specifically, the infill web plate takes a corrugated-like shape (with ridges oriented parallel to the tension stress direction) as it plastically deforms. Upon frame unloading, the infill web plate must then buckle out-of-plane as it returns to the zero-drift frame location. The corrugated infill web plate has a larger out-of-plane moment of inertia than when the infill web plate was flat (or less deformed for the case when infill web plate has already previously experienced inelastic excursions at smaller drifts), which gives rise to the compression strength observed, compared to the relatively insignificant compression strength when the infill web plate was flat;
- For frames FRB and NZB, the energy dissipation provided by the PT boundary frame is insignificant, which is expected as the boundary frame is designed to remain essentially elastic. However, some energy dissipation does appear to occur (due to effects such as friction slip in the bolted frame connections and the PT anchorages), observed by the development of minor hysteresis in the force-displacement response. Furthermore, Figs. 10(a) and 11(a) (with the superimposed PT boundary frame response) show that the contribution of base shear strength of the PT boundary frame is relatively small compared to frames with an infill web plate, which is observed to be approximately 20 to 25% for the frames tested. The base shear strength contribution of the PT boundary frame with infill web strips are proportionally larger, because the PT boundary frame strengths are identical to that of the frames with infill web plates, but less infill web plate material was provided;
- For frames FRS and NZS, the response is characteristic of a tension-only system because the hysteresis curve is nearly fully pinched at the zero-drift location. However, it is observed that there is presence of some energy dissipation at the zero-drift locations, but this is attributed to the response of the PT boundary frame as previously noted. Specifically, the unloading

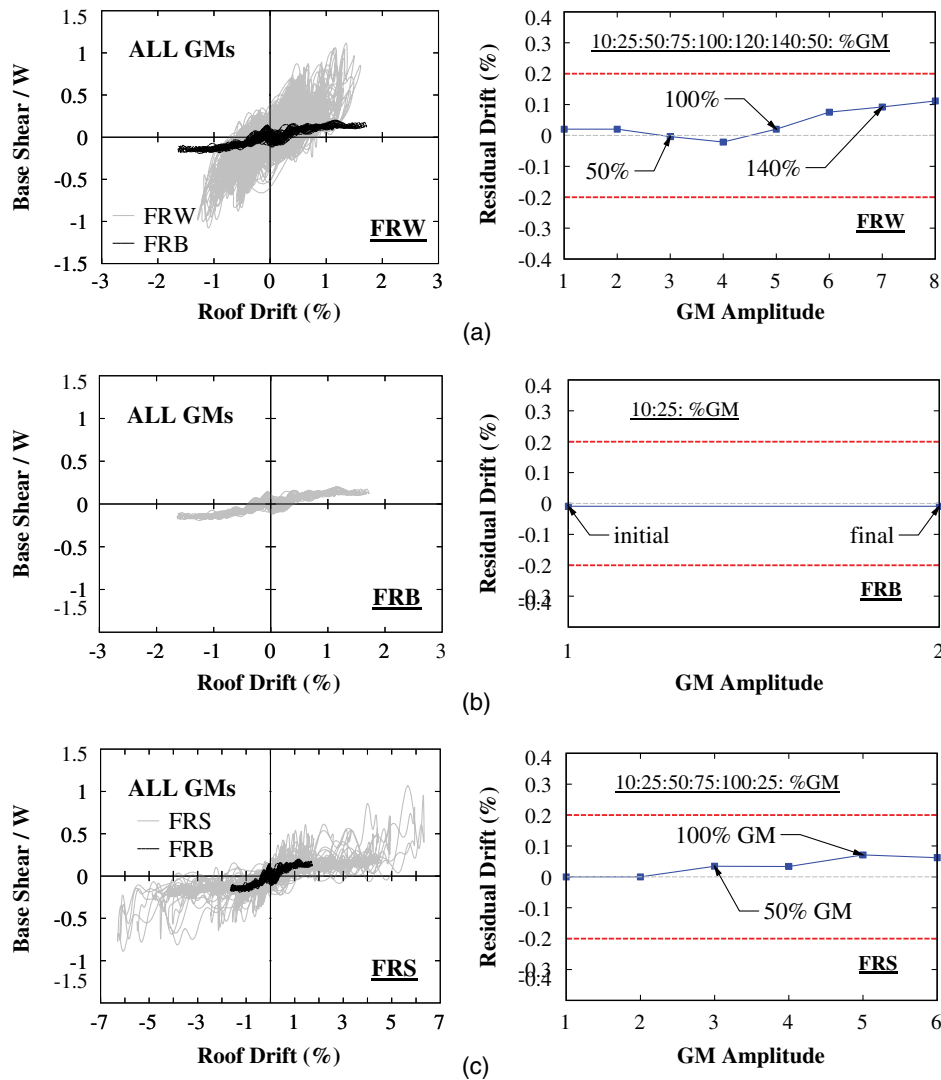


Fig. 10. Frame FR—global response: (a) FRW; (b) FRB; (c) FRS

path of frames FRS and NZS generally matches that of the corresponding frames FRB and NZB. This behavior is observed in Figs. 10(c) and 11(c) for frames NZS and FRS, respectively, where the PT boundary frame response has been superimposed for reference;

- Frame recentering was achieved for all GM amplitude tests. In particular, for frames FRW and NZW, the compression strength of the infill web plates did not affect recentering (i.e., residual drifts remained below the 0.2% threshold as noted earlier). This is attributable to the many smaller cycles of excitations that follow large cycles and occur after the out-of-plane buckling of the infill web plate has occurred. In other words, once the infill web plate buckles (as described earlier), for subsequent roof drifts that are smaller than the previous inelastic excursion, the compression stiffening effect of the deformed infill web plate on frame recentering is insignificant. While frames FRW and NZW reached peak roof drifts of approximately 1.6% and 2% drift, respectively, which could be argued to be less than the MCE drift levels, both specimens exceeded the expected DBE drift level (and the ASCE 7-10 prescribed limits of 1.5% for peak roof drifts for a steel framed building in Risk Category III as an example). Furthermore, they were subjected to multiple ground excitations, which are particularly demanding given

that, in practice, the infill web plates would be replaced after a single design level earthquake. As such, the previous observations would remain valid irrespective of drift levels; and

- To further illustrate frame recentering along the full height of the frames, Fig. 12 shows the relative (to the ground) displacement history for frames FR and NZ at each story level for the 100% GM test (which represents the design level earthquake). As observed, the recentering response is shown by the decay in story displacement and nearly perfect recentering is achieved along the frame height. For convenience, the threshold for recentering (as presented earlier) is indicated by the horizontal dashed lines in the figure, corresponding to the displacement at 0.2% drift.

Incremental Dynamic Response

The incremental dynamic response for the frames is shown in Fig. 13, where the peak absolute base shear and roof drift are plotted for each GM amplitude test. These peak values do not necessarily occur at the same point in time. Furthermore, select points are labelled corresponding to the percent GM amplitude for reference. Additionally, repeat GM amplitudes (representing earthquake aftershocks) are appended with the notation R. Also shown is the

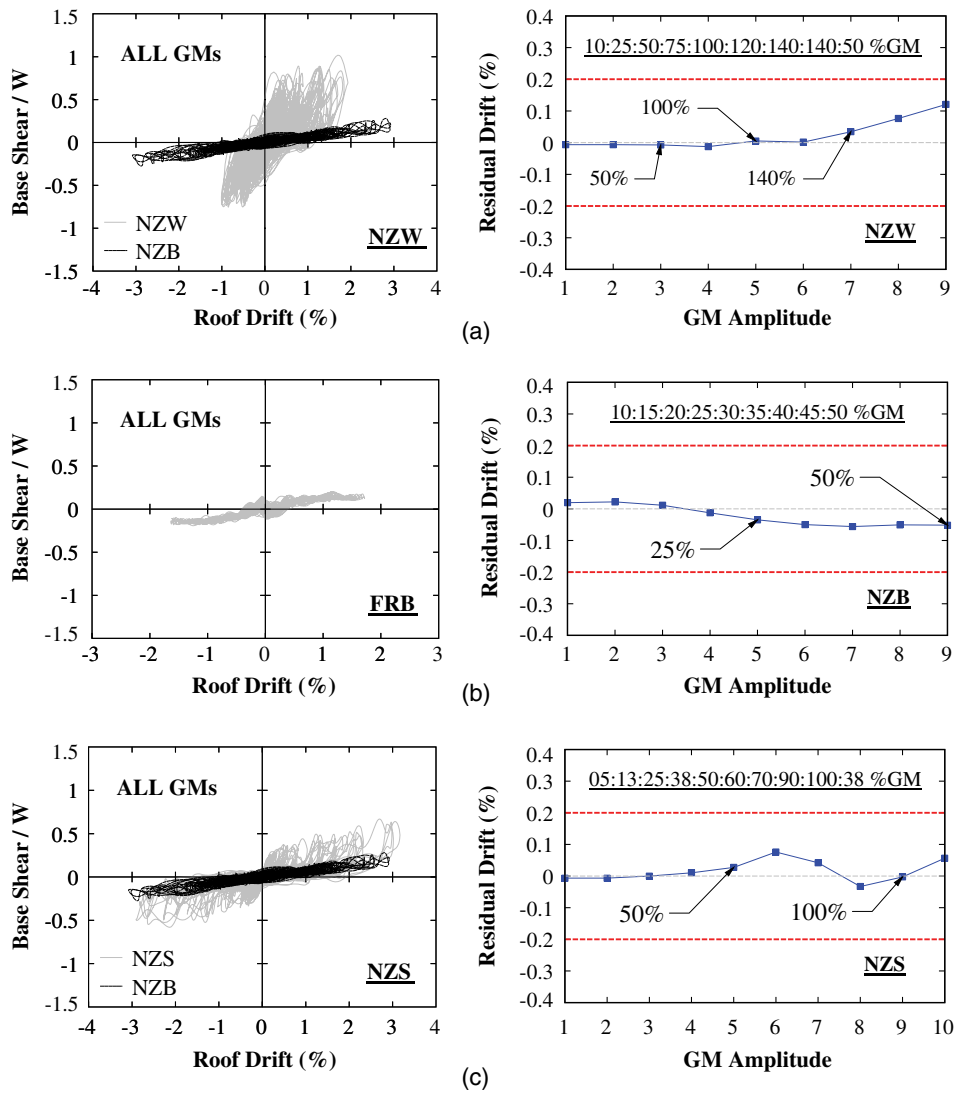


Fig. 11. Frame NZ—global response: (a) NZW; (b) NZB; (c) NZS

fundamental period for each GM amplitude test obtained from the Fourier transform transfer function of the white noise tests conducted after each GM amplitude test. Note that in Fig. 13, GM Amplitude 0 is the pretest condition of the specimen. From the incremental dynamic response results presented, the following observations are supported:

- For frame FRW, the maximum roof drift was approximately 1.6% which is relatively small compared to the 2 or 4% roof drift that one might expect for a design or maximum considered level earthquake, respectively [based on analytical studies of this structural system by Clayton et al. (2012)]. However, for perspective, recall that the prototype building was adjusted (affecting the model frame) because of operating limitations of the shake-table presented earlier. It is observed that at 75% GM indicated in Fig. 13(a), the fundamental period (obtained from white noise between seismic tests) remains constant and matches the fundamental period of frame FRB, which indicates that after significant yielding of the infill web plate the dynamic response of the frame at low amplitudes of vibration is dominated by the PT boundary frame;
- For frame FRB, it is observed that the incremental dynamic pushover response curve is bilinear, where a reduced secondary stiffness occurs when the HBE-to-VBE gap occurs. This

indicates that at the 10% GM amplitude tests, the HBE-to-VBE joints remained closed (i.e., no gap opened at the frame joints, effectively making the PT boundary frame stiffness similar to that of a rigid moment frame). The same joints opened during the 25% GM amplitude tests, producing elastic PT elongations, resulting in the secondary reduced PT boundary frame stiffness. To validate this, the PT force versus interstory drift at Level 1 is shown in Figs. 14(a and b) for the 10% and 25% GM amplitude tests, respectively. It is observed in Fig. 14(a), that the PT response curve is essentially horizontal, indicating that the HBE-to-VBE gap opening has not initiated. In contrast, in Fig. 14(b) it is shown that the HBE-to-VBE joint has opened because of the increase in PT force. A similar response was also observed at Levels 2 and 3. Furthermore, the period remained constant, indicating an elastic response, as expected of the PT boundary frame;

- For frame FRS, the maximum roof drift was approximately 6.3%, which is approximately four times that of the maximum drift corresponding to frame FRW. This was mainly attributable to the unexpected occurrence of shake-table resonance that occurred as noted at the end of this section. However, although this peak drift was likely uncorrelated to GM amplitude, this result showed that the PT boundary frame was able to fully recenter

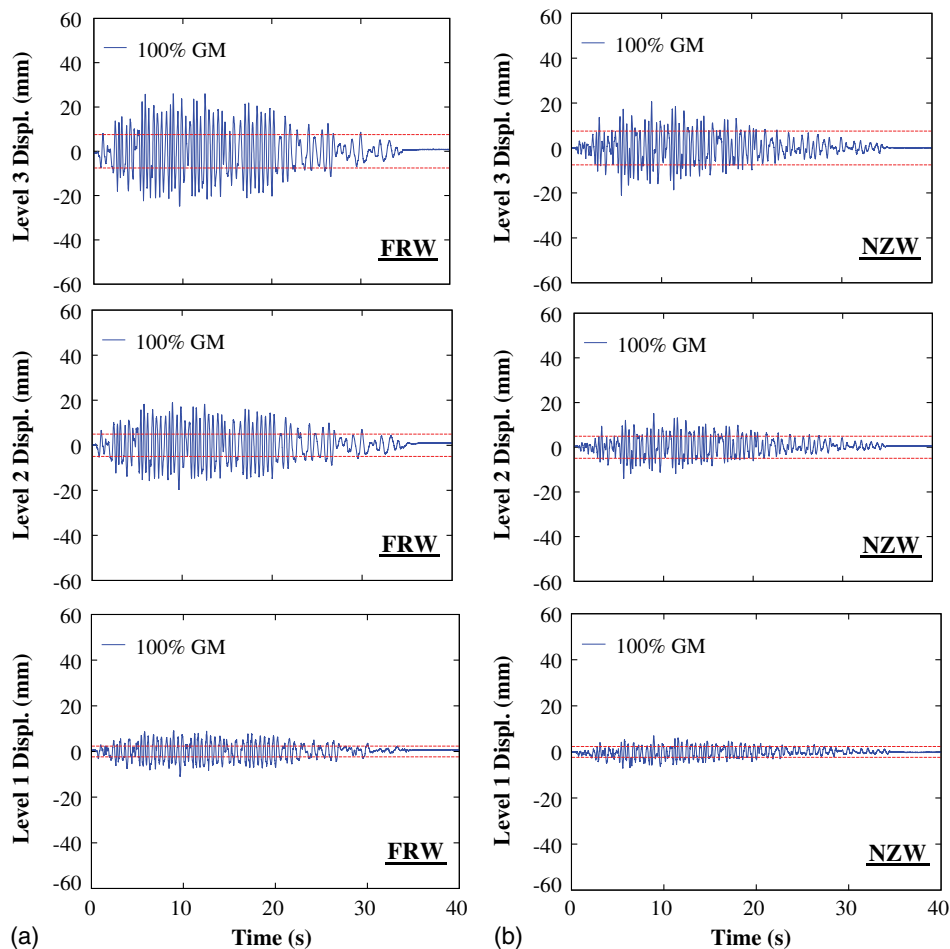


Fig. 12. Story displacement response history: (a) FRW; (b) NZW

for drift levels much larger than building drifts anticipated at design and maximum considered level earthquakes (i.e., 2% and 4%, respectively);

- For frame NZS, the maximum roof drift was approximately 3.2% at 100% GM amplitude, which is approximately 5.3 times the corresponding maximum roof drift of 0.6% for frame NZW at the same GM amplitude. Recall that the stiffness of frame NZS is approximately half that of frame NZW because of approximately 50% less infill web plate material provided by the infill web strips; and
- The maximum roof drift for frame NZB was approximately 3.1%; thus showing that the PT boundary frame response is stable at relatively large drifts. Additionally, it is observed that the incremental dynamic response curve is essentially linear, indicating that the PT strands at the closing joints remained predominately in tension (which will be clarified subsequently). Furthermore, the period remains constant, indicating an elastic response expected of the PT boundary frame.

For frames FRB and FRS, rocking resonance of the shake-table occurred because of undesired interaction with the shake-table and test specimens at the 25% GM for FRB, and 100% GM, 25% GM aftershock for frame FRS. One consequence of this is reflected in the significantly larger roof drifts compared to the results of the corresponding frames FRS and NZS [Fig. 13(c)]. The occurrence of resonance was a control issue with the shake-table drive signals and not of the specimen design. On the positive side, this resonance pushed the frame to displacements greater than originally planned, and showed that the PT boundary frame was able to fully recenter for drift levels much larger than drifts anticipated at MCE level

events, which would not have been the case if rocking resonance with the shake-table had not occurred.

Boundary Frame Posttension Response

To better understand the dynamic response of the PT HBE-to-VBE rocking joints, the PT response was investigated. In particular, it is the contribution of the PT clamping force that facilitates the ability of the joint to resist a moment (otherwise the frames would be simple pin connections with no recentering stiffness). For that reason, the PT response history was selected to provide insight into the dynamic behavior of the system, as it relates to the particular HBE-to-VBE connection (as the HBE end moment response would be similar in response but proportional to the combined effects of the story shear force, PT force, and clamping force effects from the VBES due to yielding of the infill web plates, at that level). Furthermore, reporting the PT response history is even more insightful for frame NZ, where the PT elements relax at the closing joints. Note that relax as used in the context of this paper, refers to a decrease in the initial posttensioning force, as a result of a decrease in the gap-opening below its initial value between the VBE flange and the HBE bottom flange [Fig. 4(b)] during lateral frame drift.

The concatenation of all GM amplitude results of the typical PT force versus interstory drift response is shown in Fig. 15 for the Level 1 HBEs (results for Level 2 and 3 were similar). Additionally, for specimen NZ, because the HBE PT is anchored at points within the HBE span, two PT response curves are shown. Also provided on the PT response curves are the calculated predicted response

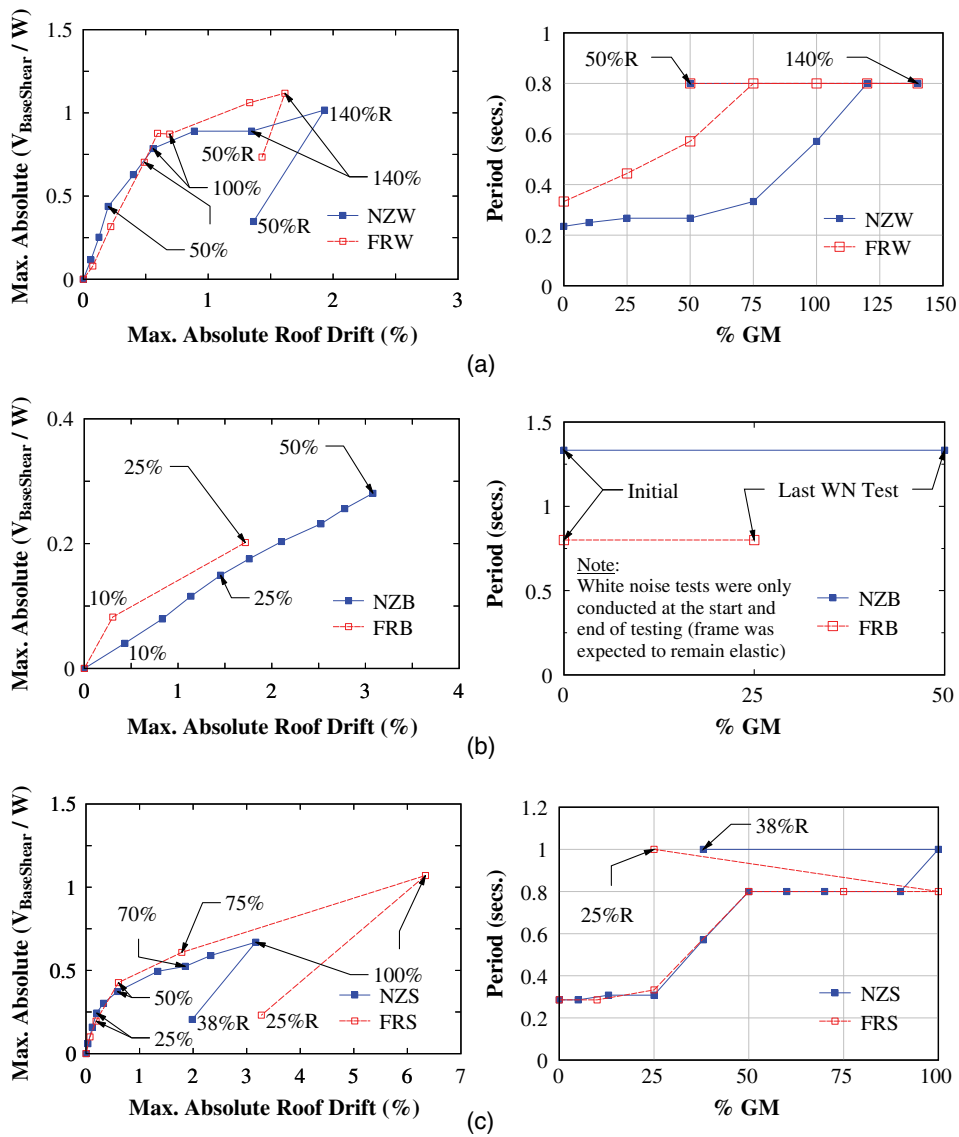


Fig. 13. Incremental dynamic response: (a) infill plate; (b) PT boundary frame; (c) infill strips

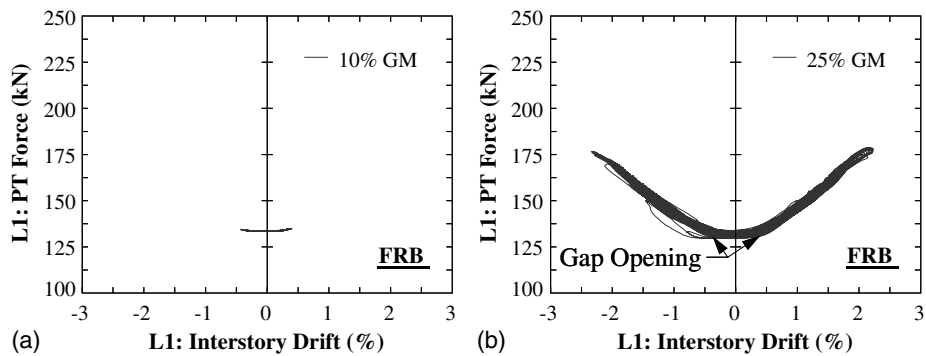


Fig. 14. Level 1 HBE PT response: (a) 10% GM; (b) 25% GM

based on analytical equations describing the PT force as a function of joint gap opening, and in the case for frame NZ, also for the condition of joint gap closing. For reference, these equations are reproduced subsequently from Dowden and Bruneau (2014), where Eqs. (1)–(3) are the PT force demands: (1) for frame FR;

(2) at the opening-joint for frame NZ; and (3) at the closing joint for frame NZ, respectively

$$P_s = P_o + \left(\frac{k_b k_{PT}}{k_b + k_{PT}} \right) \Delta_{drift} - \frac{k_{PT}}{k_b + k_{PT}} P_{HBE(VBE)} \quad (1)$$

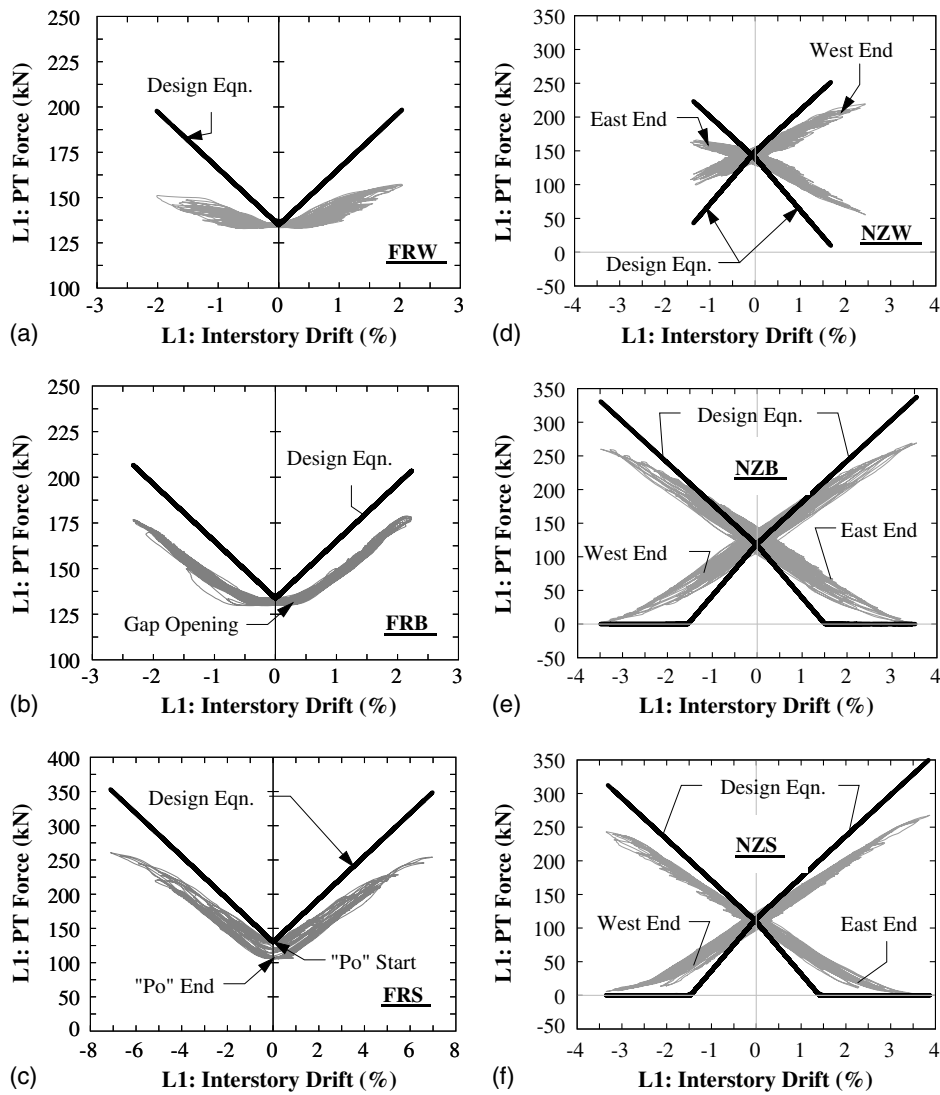


Fig. 15. Level 1 HBE PT response: (a) FRW; (b) FRB; (c) FRS; (d) NZW; (e) NZB; (f) NZS

$$P_{s1} = P_o + \left(\frac{k_{b1} k_{PT}^*}{k_{b1} + k_{PT}^*} \right) \Delta_{drift} - \frac{k_{PT}^*}{k_{b1} + k_{PT}^*} P_{HBE(VBE)} \quad (2)$$

$$P_{s2} = P_o - \left[\frac{k_{b2} k_{PT}^* + 2(k_{PT}^*)^2}{k_{b2} + k_{PT}^*} \right] \Delta_{drift} - \frac{k_{PT}^*}{k_{b2} + k_{PT}^*} P_{HBE(VBE)} \quad (3)$$

where P_o = initial posttension force; k_b = HBE axial stiffness; k_{b1} = HBE axial stiffness along length of PT at opening-joint; k_{b2} = HBE axial stiffness along length of PT at closing joint; k_{PT} = PT axial stiffness; k_{PT}^* = PT axial stiffness reduced by an amount proportional to the ratio of the PT force reaction at the HBE-to-VBE rocking point to that of the force in the PT elements; Δ_{drift} = drift induced PT elongation; and $P_{HBE(VBE)}$ = horizontal reaction at the rocking point of the yield force resultant of the infill web plate acting on the VBE. Additional information related to the previous equations and definitions can be found in Dowden and Bruneau (2014). Furthermore, the previous equations are based on the simplifying assumption that HBE-to-VBE joint rotation is equal to the roof drift ratio (i.e., rigid boundary frame response). From the results presented in Fig. 15, the following observations are supported:

- For frame FR, there is an initial transition near the zero-drift axis where the PT force remains relatively constant; this is more clearly observed in frame FRB. This transition is associated with a delay in gap opening, which at incipient initiation defines the HBE-to-VBE joint decompression moment. Prior to the joint gap opening, the response of the connection is comparable to that of a rigid moment connection;
- For frame FRW, it is shown that the PT response appears to be nonlinear (i.e., loading and unloading do not follow the same load path), even though the PT elements remained elastic. In part this is attributable to the abrupt and erratic dynamic loading (recognizing this may lead to some noise in the data) and a contribution of nonlinear response due to PT force losses (i.e., because of anchor wedge seating, HBE elastic shortening, etc.), but is also due to the effects of the infill web plate pulling on the PT boundary frame through tension-field action. In doing so, the HBE-to-VBE joint rotations (affecting the PT elongations) will be affected because of the flexibility of the HBEs and VBEs. In comparison with frame FRB, with the absence of infill web plates, the PT response for frame FRB is essentially bilinear elastic (i.e., defined by an initial stiffness prior to HBE-to-VBE gap opening and a secondary reduced stiffness after HBE-to-VBE gap opening);

- For frame FRS, it is shown that the PT response appears to be nonlinear. Given that infill web strips behave as essentially tension-only elements (as observed earlier), the response would be expected to be bilinear elastic. However, the occurrence of the abrupt increase in roof drift [i.e., between the 75 and 100% GM shown in Fig. 13(c)], resulted in an increase in PT force losses. This is shown by the downward vertical shift of the PT force along the vertical axis (at zero-drift), as noted in Fig. 15(c) (where P_o Start and P_o End refers to the start and end of the test series, respectively). If PT force losses had not occurred the response would have been similar to that of frame FRB (i.e., bilinear elastic). To provide further clarification, Fig. 16(a) presents the cumulative PT force response for tests conducted up to 75% GM, which shows an essentially bilinear elastic response. Rocking resonance occurred with the shake-table at the following 100% GM test, where the maximum roof drift was approximately 6.3%, an increase of 3.5 times that of the

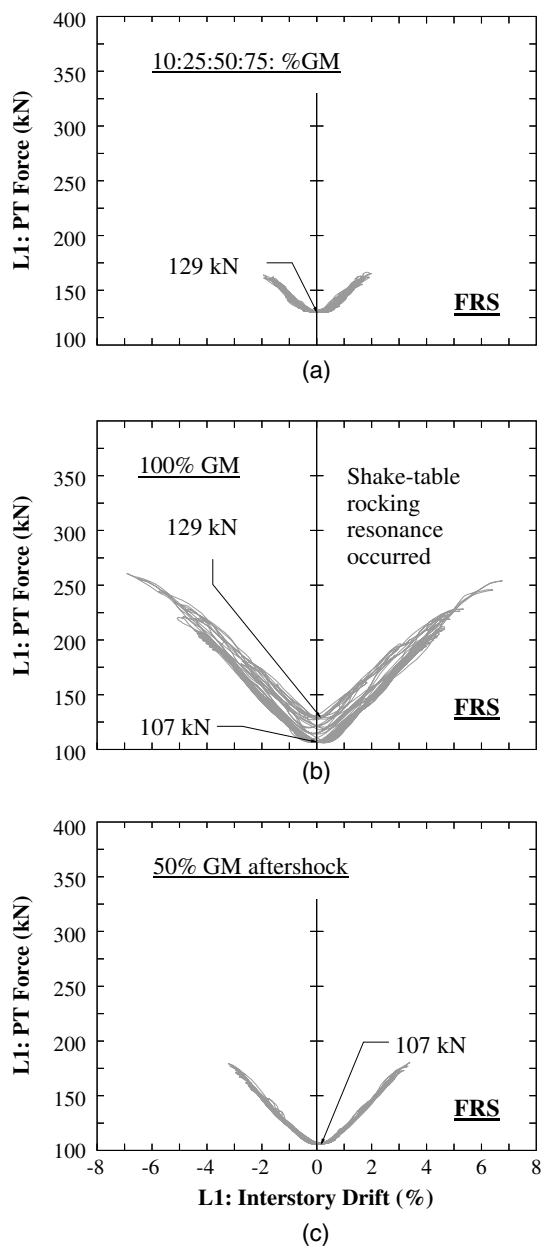


Fig. 16. Level 1 FRS HBE PT response: (a) 10 to 75% GM; (b) 100% GM; (c) 50% GM repeat

1.7% roof drift that occurred for the prior 75% GM test. As shown in Fig. 16(b), this led to a reduction in initial PT force of approximately 22 kN (5 kips). Thus, the appearance of hysteretic behavior in Fig. 16(b) is attributable to losses in the initial PT force and not because of yielding of the PT elements. For the concluding 50% GM test, no appreciable losses in PT forces occurred as evidenced by the bilinear elastic response shown in Fig. 16(c);

- For frame NZW, an immediate increase of PT force occurs at the opening-joint locations due to the presence of an initial gap at the bottom of the HBE flanges (for the reason that no decompression moment is present compared to frame FR). Correspondingly, at the closing joint locations, a decrease in PT force occurs. For the condition shown, a maximum interstory drift of approximately 2.3% was achieved and the PT at the closing joint did not become fully relaxed. Furthermore, for reasons noted for frame FR, the PT force response are nonlinear because of the effects of the infill web plates and PT force losses between GM amplitude tests;
- For frame NZB, it is shown that the PT response appears to be nonlinear. But given that there is no infill web plates/strips installed for this specimen, the response would be expected to be bilinear elastic (i.e., defined by an initial stiffness prior to full relaxation of the PT elements at the HBE-to-VBE closing joints and a secondary reduced stiffness at complete relaxation of the PT elements at the HBE-to-VBE closing joints). However, as indicated by the incremental dynamic pushover curve in Fig. 13(b), nine shake-table tests were conducted on that specimen. Thus, the effect of conducting many dynamic tests on the specimen may have had a dominant influence on PT force losses due to PT anchor wedge seating (then attributing to the hysteretic like response shown as described in observation #3 previously). Additionally, because the PT elements are relatively short for frame NZ (e.g., compared to frame FR), the PT force losses will be more prominent. Furthermore, it is shown that complete PT relaxation occurred at large drifts. In doing so, the PT anchors may have experienced some vertical slip, which may have had some increased effect on the PT force losses;
- For frame NZS, it is shown that the PT response appears to be nonlinear. Given that infill web strips behave as essentially tension-only elements (as observed earlier), the response would be expected to be bilinear elastic. Also, given that the peak roof drift was approximately the same as that observed for frame NZB and that no changes to the PT elements were made between test setups, additional PT force losses from anchor wedge seating would be expected to be insignificant. However, it is shown that eventually for large drifts, complete relaxation of the PT elements occurred. Accordingly, PT force losses due to vertical slip of the PT anchors may have occurred for reasons just presented earlier. This could have been prevented by welding the PT anchors to the HBE anchor plate or by using any other similar type of detailing to keep the PT anchor plates in place. Furthermore, although complete PT relaxation occurred at the HBE-to-VBE closing joint locations, this did not have an effect on the recentring response observed in Fig. 11(c); and
- In a comparison of the experimental versus predicted PT response, the simplifying assumption used in the analytical predictions that the HBE-to-VBE joint rotation is equal to roof drift ratio provides an upper-bound estimate of PT force. Additionally, the analytical equations are also conservative for the reason that PT force losses due to anchor wedge seating and flexibility of the VBEs are not accounted for. Furthermore, for frame NZ, the analytical equations conservatively show full relaxation at

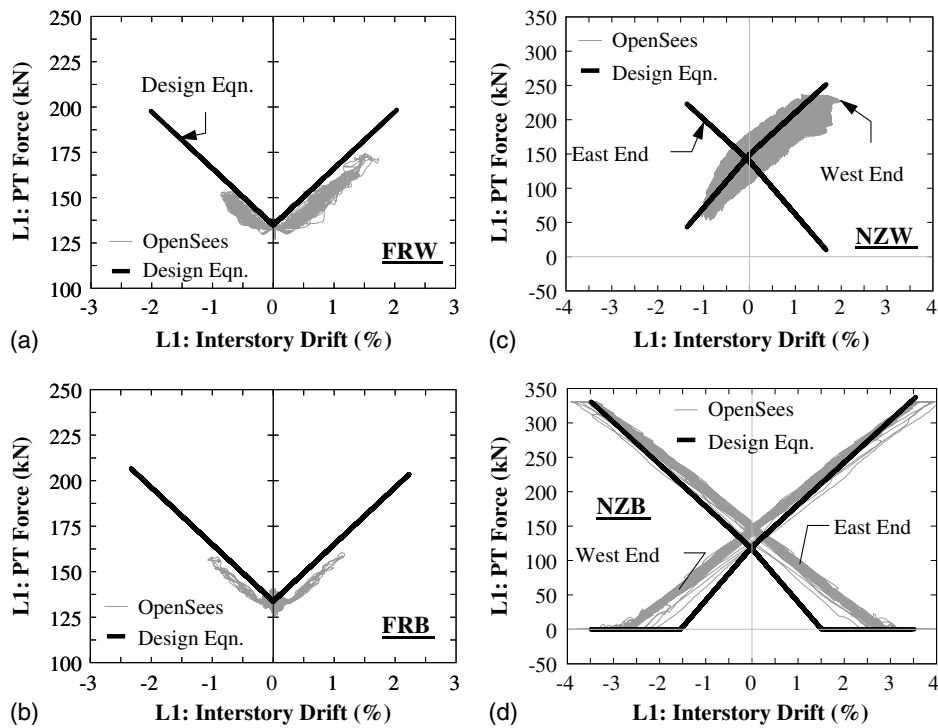


Fig. 17. Level 1 HBE PT results using design equation compared to OpenSees: (a) FRW; (b) FRB; (c) NZW; (d) NZB

the PT elements at the closing joint at lower drifts than the experimental data. However, the differences between the analytical predictions and the experimental responses are not negligible. To provide some explanation, Fig. 17 shows the analytical prediction values overlaid with nonlinear dynamic response history analyses from *OpenSees* (details of which will be presented later). For this purpose, the numerical model assumed 5% damping and used a tension-only infill web strip model. As shown in the figure, the differences between the experimental versus analytical comparisons are less, but some noticeable differences still remain. This suggests that the numerical model does not fully capture the actual flexibility of the test specimen and in particular, the HBE-to-VBE connections. In part, this could be because of the nodal constraints used to transfer HBE shears to the VBEs (in the numerical model that will be presented in a later section), whereas in the actual connection some flexibility is provided by the shear plate connection (Fig. 4). Similarly, the analytical equations are conservative as the derivations were based on the kinematics of a rigid frame with idealized pinned connections (Dowden and Bruneau 2014). Nonetheless, the results show that the analytical equations and the numerical model presented subsequently provide an upperbound approach for estimating the PT demands for design (which is what is required for design purposes).

Infill Web Plate Tensile Strains

The HBE-to-VBE connections of SC-SPSWs are detailed with a cut-out at the infill web plate corner locations as shown in Fig. 4. The primary purpose of this detail is to remove the portion of the infill web plate at the infill web plate corner locations that would otherwise be subjected to excessive tensile strains during lateral frame drift due to the opening of the rocking joint. That is, in addition to the tensile strains resulting from a panel sway mechanism,

compounding strain effects are also present due to the formation of a gap at the HBE-to-VBE joint. Use of corner cut-outs in the infill web plate is essential at the HBE-to-VBE joint detail to avoid large tensile strains at these locations, which could lead to a premature unzipping effect of the infill web plate tearing from the boundary frame. Dowden and Bruneau (2014) presented an analytical relationship that accounts for this behavior describing the total tensile strain on the infill web plate for HBE-to-VBE rocking connections at a distance R_{cutout} away from the HBE-to-VBE flange rocking point as follows:

$$\varepsilon_{\text{Total}} = \frac{\gamma \sin 2\alpha}{2} \left(\frac{d}{R_{\text{cutout}}} \frac{\tan \alpha + \cos \alpha + \sin \alpha \tan \alpha}{\cos \alpha + \sin \alpha \tan \alpha} \right) \quad (4)$$

where R_{cutout} = radius length of the corner cut-out; α = angle of inclination of the tension field to the vertical axis; d = depth of the HBE; and γ = HBE-to-VBE relative gap opening rotation in units of radians. In Eq. (4), the bracketed term is a magnification factor as a result of the HBE-to-VBE gap opening. If $R_{\text{cutout}} = 0$ (i.e., an infill web plate corner cut-out is not provided), the theoretical tensile strain at that location is infinite, which would cause early fracture of the infill web plate at the corners. This could have a cascading effect by facilitating further infill web plate fracture because of propagation of this initial tearing of the infill web plate from the boundary frame, although future research would be required to ascertain the severity of this consequence and how it would impact behavior.

To check the accuracy of Eq. (4), Fig. 18 shows diagonally placed string potentiometers that were provided along the infill web plate on the test specimens. In that figure, the sensors were placed at 45 degrees with the vertical at a corner cut-out location (i.e., a radial corner cut-out of approximately 203 mm or 8 in.), near the corner cut-out, and a distance far removed from the corner cut-out for the Level 1 HBE with sensor names spwpn1, spwpn2, and spwpn3, respectively. The experimental versus analytical axial

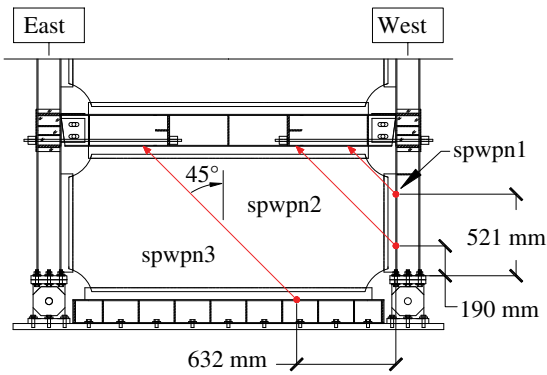


Fig. 18. Infill web plate string pots

deformation response for frame FRW and NZW at these locations are provided in Fig. 19. From the comparisons shown, the experimental and analytical results compare reasonably well. However, it is observed that there is an increased difference with the results at

spwpn3 compared to the other two locations. In particular, the tensile elongation measurements recorded by spwpn3 were larger than those calculated using the analytical equation. But from Fig. 18 the displacement transducer at one end was connected to the foundation level anchor beam, which is essentially a fixed point. In contrast, the displacement transducers spwpn1 and spwpn2 were attached to the VBE, which is allowed to rotate. The derivation of Eq. (4) is based on the boundary conditions of spwpn1 and spwpn2. Accordingly, the results show that Eq. (4) can be used to inform design in establishing an appropriate value of the corner cut-out radius (i.e., the location of spwpn1).

Numerical Modeling

Numerical models of the SC-SPSW frames were developed using the program *OpenSees* (Mazzoni et al. 2009). The boundary frame members, infill web plates, and posttension materials were ASTM A992 (ASTM 2015c), ASTM A1008 (ASTM 2015b), and ASTM A416 (ASTM 2015a), respectively. A strip model approach (Sabelli and

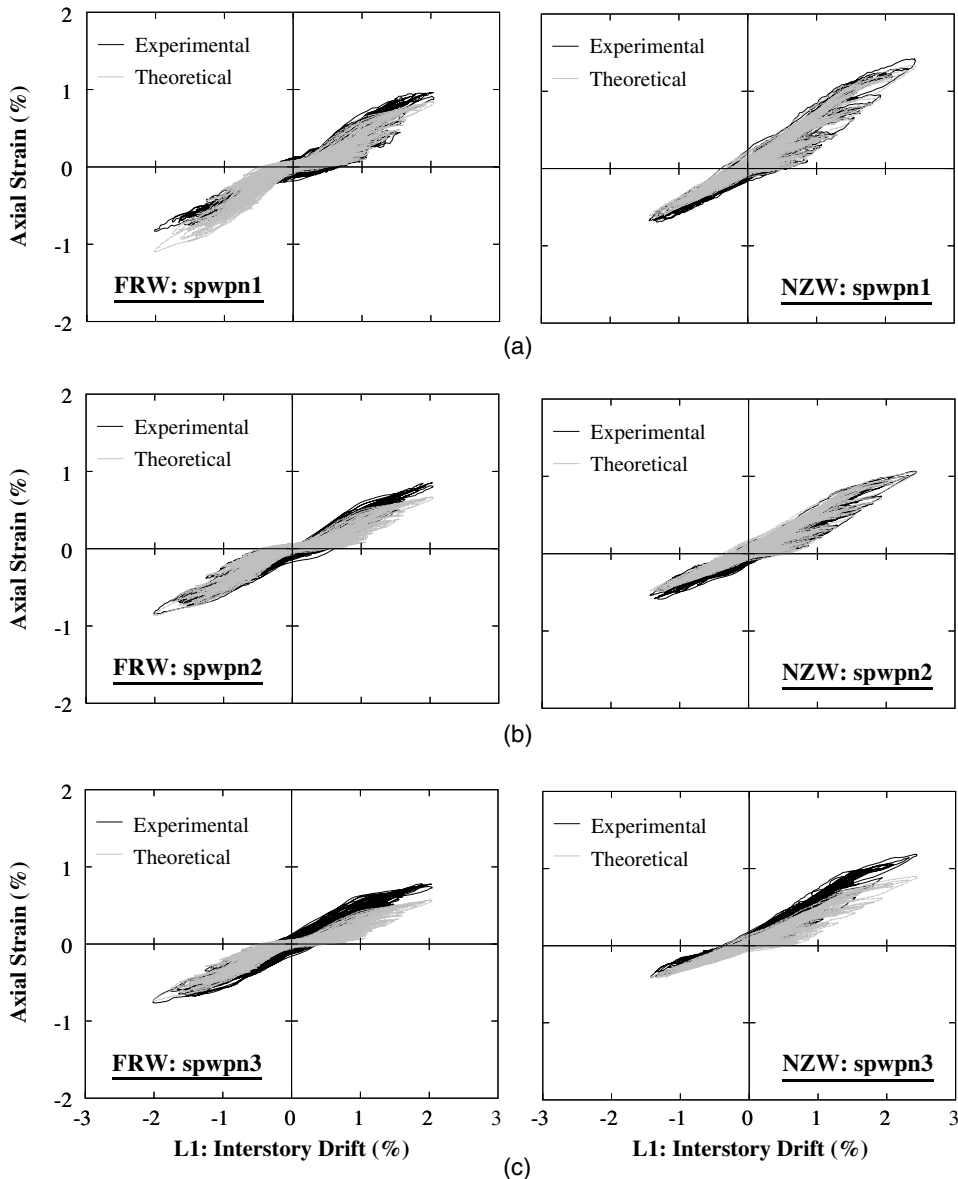


Fig. 19. Frame FRW and NZW experimental versus theoretical at displacement transducer: (a) spwpn1; (b) spwpn2; (c) spwpn3

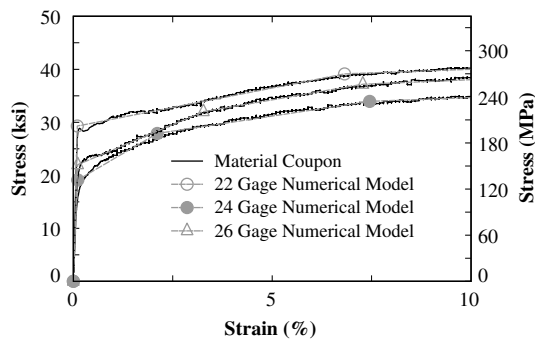


Fig. 20. Infill web plate coupon tension test results

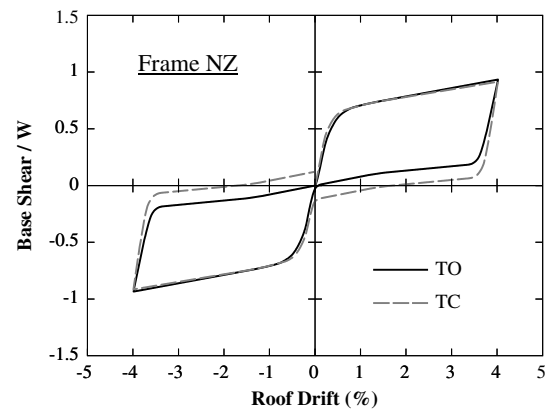


Fig. 21. OpenSees inelastic cyclic pushover

Bruneau 2007) was used to model the SPSW infill web plate. Accordingly, the infill web plate was modeled using a series of truss elements/strips, where each strip element was assigned an axially yielding member model using the *Hysteretic Material* definition to account for nonlinear hysteretic behavior. In particular, the material definition has a user option of a *pinchx* and *pinchy* factor that provides pinching for strain and stress during reloading, respectively. To model tension-only behavior of the infill web plates, values of 1.0 and 0.0001 were used for those factors, respectively. Furthermore, the backbones of the axially yielding elements were calibrated with material coupon tests taken from each batch of the infill web plates used in these tests and results presented in Fig. 20. The stress-strain data presented in that figure can be downloaded from the NEES repository. Furthermore, both a tension-only (TO) and a simplified combined tension-compression (TC) hysteretic model for the infill web strips was considered, where the TC model considers some constant compression strength contribution of the infill web plate. To facilitate the latter, the *Elastic-Perfectly Plastic* and *Hysteretic Material* definitions were combined using the *Parallel Material* definition offered by *OpenSees*. For this purpose, the *Hysteretic Material* component is identical to that used in the TO model and the *Elastic-Perfectly Plastic* component is modeled as compression-only behavior. This simplified TC model approach was proposed by Clayton (2013) where a more detailed presentation on the TC model is provided. Note that the TC model used to capture the effects of the infill web plate compression is not a true representation of the actual behavior, but rather an approximate method to account for some of the compression strength observed in previous quasi-static cyclic tests of SC-SPSWs (Winkley 2011; Clayton 2013; Dowden 2014).

Furthermore, based on calibration of the numerical models with the experimental results from the previous conducted quasi-static cyclic tests on the same test specimens (Dowden and Bruneau 2014), the compression strength assigned to the *Elastic-Perfectly Plastic Material* component in the numerical model was found to be approximately 20% of the tensile yield strength of the infill web plate. The 20% value was used in order to obtain an accurate comparison of the numerical experimental base shear versus roof drift results with the quasi-static cyclic test results. However, the actual percent value could be as low as 10% as reported by Dowden and Bruneau (2014). In particular, the numerical model is a frictionless idealized representation of the test specimen. The 20% value used in the numerical model (for the purpose of calibration) then lumps any strength effects due to the specimen interaction with the experimental setup (e.g., diaphragm load transfer to the specimen, any restraining effects of the test setup, etc.) and the various parts within the specimen (e.g., connection details, construction tolerances, presence of friction at the beam-column joints and at diaphragm connections, etc.) into the numerical

model. Because the shake-table tests used the identical test setup as the previously conducted quasi-static tests (against which the numerical models were calibrated), these calibrated models were deemed appropriate for use with the numerical simulations for the shake-table tests.

To illustrate the hysteretic response described previously, Fig. 21 shows a comparison of the TO and TC numerical model inelastic force-displacement cyclic response for frame NZ (with an infill web plate), arbitrarily shown for a 4% roof drift. As shown in that figure, for a rightward drift direction, the TC infill web plate model matches the TO model, and on the unloading cycle back to zero-drift, some compression strength of the infill web plate is developed. Furthermore, from observation of the TC model results, it is observed that the frame recentering response is affected by the compression strength of the infill web plates for static cyclic loading conditions, and that at the zero base shear location, a non-negligible residual drift occurs. However, as presented earlier, the experimental data show that frame recentering occurs for dynamic loading conditions contrary to the TC model response shown in the figure.

The PT elements were modeled using truss elements. The yield strength of the PT elements was assumed to be 90% of the ultimate tensile strength of the PT material and the elastic modulus was assumed to be 200 GPa (29,000 ksi). For frame FR, these elements were modeled with the *Steel02 Material Giuffre-Menegotto-Pinto Material* definition with a strain hardening ratio of 0.02. To simulate the initial applied PT force, the user option of providing an initial stress value was used. For frame NZ, the PT elements use the *Elastic-Perfectly Plastic Gap Material* definition with no strain hardening, which allows for tension-only behavior. Recall that for the NZ connection, PT elements at the closing joint locations will relax. This latter material definition simulates that behavior, which also allows a user input of an initial negative strain to simulate the initial applied PT forces. Additionally, the PT elements were designed to remain essentially elastic. Therefore, for this purpose, an elastic-perfectly plastic material definition for the PT elements was deemed acceptable. The rocking connection was modeled using compression-only springs (using the *Elastic-No Tension Material* definition) at the HBE-to-VBE contact flange locations in combination with the use of nodal constraints and *rigidlink beams*. The numerical models of the test specimens and rocking joints are shown in Figs. 22 and 23, respectively. Note that in Fig. 22, infill web strips are shown near the corner cut-outs, which are not identical to the actual detailed corner radius of the test specimens shown in Fig. 4 (i.e., to prevent early fracture of the infill web plate at the corners as noted earlier). However, the analytical

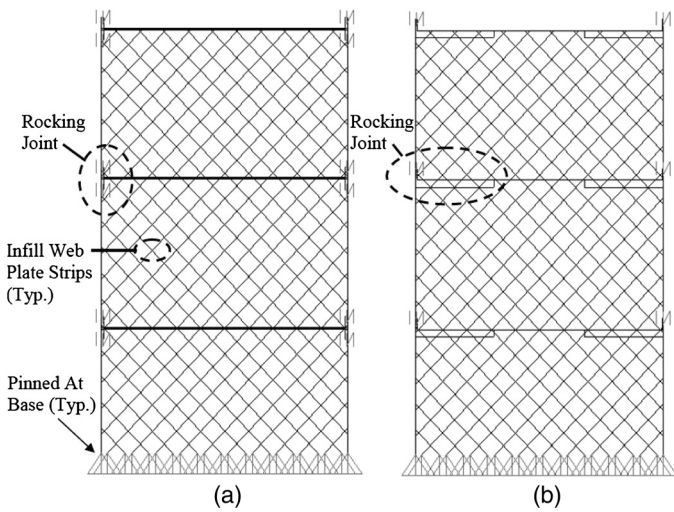


Fig. 22. Numerical models: (a) frame FR; (b) frame NZ

strip model is a simplified model intended to capture the overall behavior of the plate as a continuum. The corner cut-out is an insignificant part of the plate continuum, such that a refined level of accuracy in detailing the strip model is unwarranted and of little consequence on the numerical results. The coupon tension tests for the boundary frame members and PT strands were not performed as it was expected that these components would remain essentially elastic.

Finally, for the nonlinear dynamic response history analyses, the total seismic weight of 76 kN (17 kips) per floor level was equally distributed at the ends and at midpoint of each corresponding HBE as lumped masses. These locations correspond to the diaphragm connection points along the HBEs in the test setup, as shown in Fig. 7. Equivalent viscous damping was modeled in the form of mass proportional damping, proportional to the first mode period. Furthermore, a time step of 0.001 seconds was used for the nonlinear response history analyses. Additional information on the numerical modeling is provided in Dowden and Bruneau (2014).

Comparison of Numerical and Experimental Results

The incremental dynamic pushover (i.e., maximum absolute base shear versus peak roof drift) response from *OpenSees* analyses, using the identical GM sequence of the test specimens, was compared with the experimental results, where the numerical results for frames FRW, NZW, FRS, and NZS are presented in Fig. 24 for a lower bound and upper bound equivalent linear viscous damping ratio of 2% and 5%, respectively. Furthermore, both TO and TC responses of the infill web plate models were considered. Also, each point on the numerical incremental dynamic curve includes the cumulative inelastic deformation history from the previous scaled GMs (as was the case for the experimental results); this was done by concatenating the appropriate scaled GMs and providing a segment of free vibration between each GM to approximately reset the initial velocity and acceleration conditions to zero between GMs (as would be the case for the shake-table tests).

The numerical versus experimental incremental dynamic response curves for frames FR and NZ are presented in Figs. 25(a and b), respectively. The comparison results are made only up to the largest intensity GM as noted in the figure (i.e., repeat GMs and aftershock GMs are not included). For clarity, only results for the numerical model for each TO and TC damping condition that best compares with the experimental results are shown superimposed in the figure. From the comparisons shown, the TO model with large damping (i.e., 5%) and the TC model with low damping (i.e., 2%) provide results comparable to the experimental ones. Additionally, for the frames with infill web strips, the TO model with small damping (i.e., 2%) provides the best comparison. Furthermore, it is observed that the comparisons with the infill web strips, in general, provide a better match to the experimental results than those of the corresponding frames with infill web plates. This provides further evidence that the infill web strips are tension-only. From the results shown, the numerical models are able to provide a reasonable prediction of the absolute maximum base shear and peak roof drift demands for the bounded conditions of the equivalent linear viscous damping ratios used in the numerical analyses.

Note that some other researchers have also previously reported on the contribution of compression strength to the total infill web plate strength (Driver et al. 1997), and proposed a modified strip

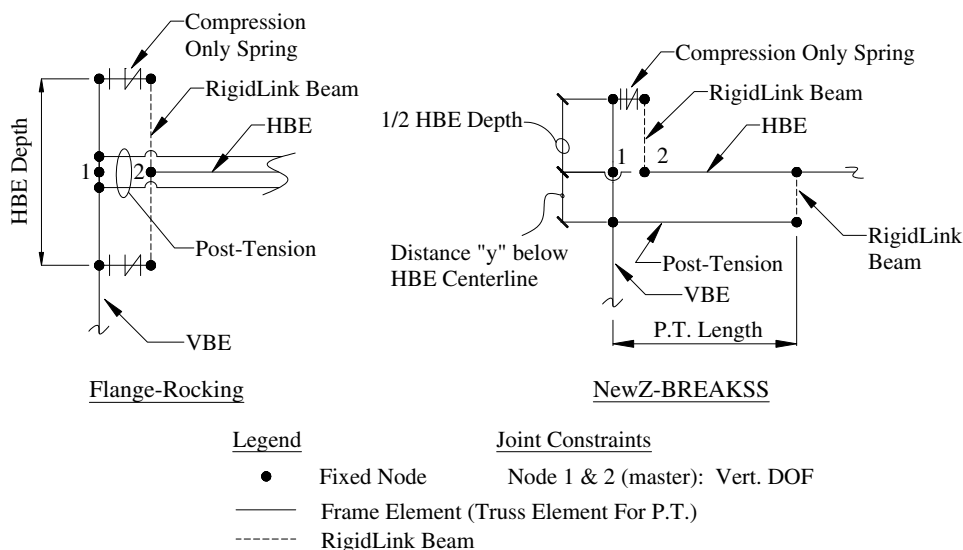


Fig. 23. Numerical model—joints

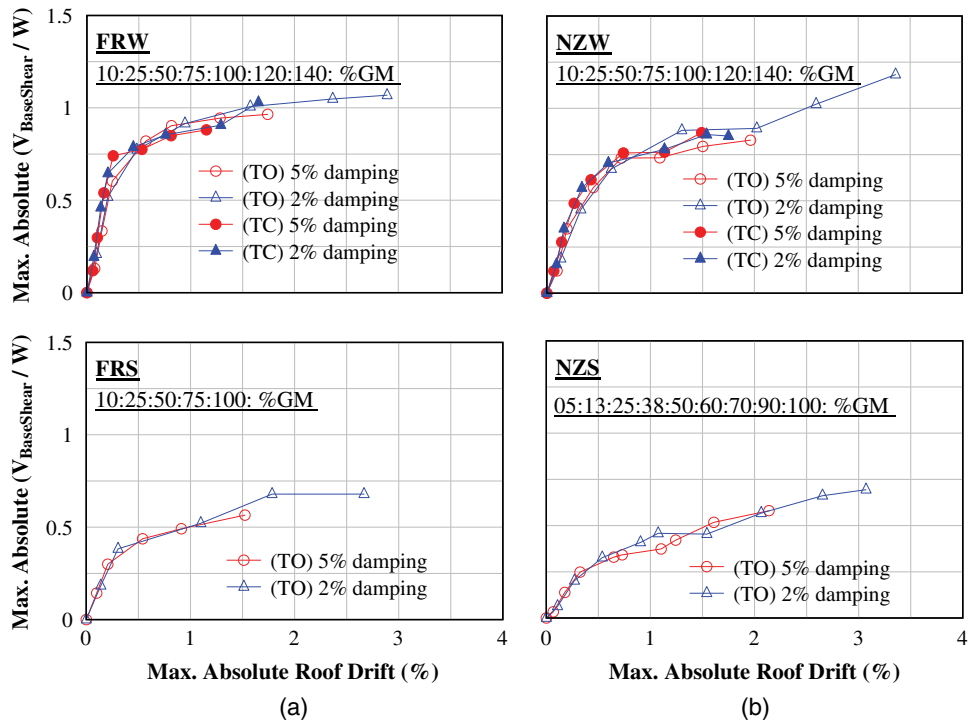


Fig. 24. OpenSees numerical IDR: (a) frame FR; (b) frame NZ

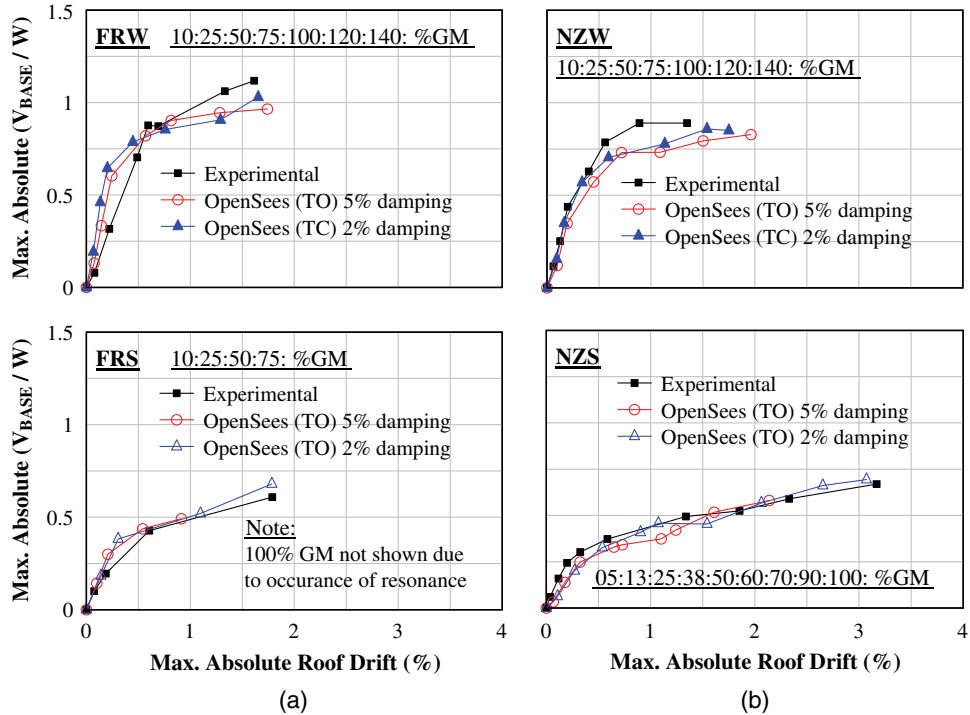


Fig. 25. Experimental versus numerical IDR: (a) frame FR; (b) frame NZ

model (Shishkin et al. 2009) to consider this compression strength in SPSW analysis. More recently, Webster (2013) proposed a new *OpenSees* uniaxial material model (not available at the time of the research reported in this paper), specifically developed to replicate the compression effect due to infill web plate buckling observed in

SPSWs under cyclic loadings. However, the previous model (i.e., Webster 2013), based on calibration to results from limited cyclic tests and finite element analyses, remain to be substantially validated with experimental results for SPSWs subjected to dynamic earthquake loadings.

Summary and Conclusions

This paper presented the results of a shake-table test program conducted on self-centering steel plate shear walls. Specimens consisted of one-third scaled, single-bay, three-story frames detailed with a flange-rocking and the newly proposed NewZ-BREAKSS HBE-to-VBE PT rocking joint connections. In the former detail, joint gap opening is provided through rocking about the top and bottom HBE flanges, whereas in the latter, an initial gap is provided at the HBE bottom flanges and the HBE rocks only about the top flanges, essentially eliminating PT boundary frame expansion that occurs with the former rocking connection. The experimental base shear versus roof drift results were presented and showed that both SC-SPSW types achieved self-centering, while validating the use of replaceable energy dissipation elements in this type of lateral force resisting system. Insights on the connection kinematics were provided through the results of the experimental posttension versus interstory drift response. In particular, for the NewZ-BREAKSS connection, complete relaxation of the PT elements at the closing joints occurred and did not have a detrimental effect on the SC-SPSW response.

Numerical models were developed in the program *OpenSees*, where nonlinear response history analyses were performed. The results were presented in an incremental dynamic pushover format (presenting only the absolute predicted maximum base shear and peak drifts) and were comparable to the experimental results. Additionally, the experimental PT force response was compared to predicted response, based on analytical equations derived from the kinematics of the PT rocking joints; this showed that the analytical equations provide a conservative prediction suitable for initial PT design. Furthermore, an important consideration of the HBE-to-VBE joint connection is detailing the infill web plate with corner cut-outs. The purpose of this detail is to remove the portion of the infill web that is subjected to large tensile strains due to the gap opening at the HBE-to-VBE rocking joints. An analytical equation was presented to calculate strains at the infill corner for boundary frames detailed with HBE-to-VBE rocking connections. As shown by that equation, if the radius of the corner cut-out was zero (i.e., no cut-out provided), the theoretical tensile strain at that location would be infinite. Displacement transducers were installed on the test specimens to investigate the deformation response of the infill web plate and recorded values were compared to those predicted by the analytical relationship. The comparisons with the experimental and analytical results were in good agreement.

The experimental investigation provided key insights into the seismic response of SC-SPSW systems that would not otherwise be fully realized with conducting only cyclic static loading tests. In particular, recentering was found to not be sensitive to the compression stiffening of the infill web plate, contrary to what had been initially observed in the quasi-static test phase. In part, this is because of the many smaller cycles of excitations that follow the larger cycles after the temporary compression strut effect develops. These smaller cycles occur on infill web plates having less structured out-of-plane buckling shapes that offer less compression resistance than the corrugated plate effect that develops when new inelastic excursions exceed previously reached ones. The results presented show that SC-SPSWs can be repaired, provide frame recentering, and minimize structural damage of the gravity frame components of the lateral force resisting system. SC-SPSWs thus offer enhanced structural performance (beyond conventional lateral systems) and would be appropriate for buildings in regions of high seismicity.

Acknowledgments

Financial support for this study was provided by the National Science Foundation as part of the George E. Brown Network for Earthquake Engineering Simulation under award number CMMI-0830294. Additional financial support for D. Dowden was provided by MCEER. Any opinions, findings, conclusions, and recommendations presented in this paper are those of the authors and do not necessarily reflect the views of the sponsors.

References

- AISC. (2005). "Seismic provisions for structural steel buildings." *ANSI/AISC 341-05*, Chicago.
- AISC. (2010). "Seismic provisions for structural steel buildings." *ANSI/AISC 341-10*, Chicago.
- ASCE. (2010). "Minimum design loads for buildings and other structures." *ASCE/SEI 7-10*, Reston, VA.
- ASTM. (2015a). "Standard specification for low-relaxation, seven-wire steel strand for prestressed concrete." *ASTM A416/A416M-15*, West Conshohocken, PA.
- ASTM. (2015b). "Standard specification for steel, sheet, cold-rolled, carbon, structural, high-strength low-alloy, high-strength low-alloy with improved formability, solution hardened, and bake hardenable." *ASTM A1008/A1008M-15*, West Conshohocken, PA.
- ASTM. (2015c). "Standard specification for structural steel shapes." *ASTM A992/A992M-11*, West Conshohocken, PA.
- Christopoulos, C., Filiatrault, A., Uang, C. M., and Folz, B. (2002). "Post-tensioned energy dissipating connections for moment-resisting steel frame." *J. Struct. Eng.*, 10.1061/(ASCE)0733-9445(2002)128:9(1111), 1111–1120.
- Clayton, P. M. (2013). "Self-centering steel plate shear wall: Subassembly and full-scale testing." Ph.D. dissertation, Dept. of Civil and Environmental Engineering, Univ. of Washington, Seattle.
- Clayton, P. M., Berman, J. W., and Lowes, L. N. (2012). "Seismic design and performance of self-centering steel plate shear walls." *J. Struct. Eng.*, 10.1061/(ASCE)ST.1943-541X.0000421, 22–30.
- Clifton, G. C., MacRae, G. A., Mackinven, H., Pampanin, S., and Butterworth, J. (2007). "Sliding hinge joints and subassemblies for steel moment frames." *Proc., New Zealand Society of Earthquake Engineering Annual Conf.*, Palmerston North, New Zealand.
- Dowden, D. M. (2014). "Resilient self-centering steel plate shear walls." Ph.D. dissertation, Dept. of Civil and Environmental Engineering, Univ. at Buffalo, Buffalo, NY.
- Dowden, D. M., and Bruneau, M. (2011). "NewZ-BREAKSS: Post-tensioned rocking connection detail free of beam growth." *Eng. J.*, 48(2), 153–158.
- Dowden, D. M., and Bruneau, M. (2014). "Analytical and experimental investigation of self-centering steel plate shear walls." *Tech. Rep. MCEER-14-0010*, Multidisciplinary Center for Earthquake Engineering Research, State Univ. of New York Buffalo, Buffalo, NY.
- Driver, R. G., Kulak, G. L., Kennedy, D. J. L., and Elwi, A. E. (1997). "Seismic behavior of steel plate shear walls." *Structural Engineering Rep. 215*, Dept. of Civil Engineering, Univ. of Alberta, Edmonton, AB, Canada.
- Erochko, J., Christopoulos, C., Tremblay, R., and Kim, H.-J. (2013). "Shake table testing and numerical simulation of a self-centering energy dissipative braced frame." *Earthquake Eng. Struct. Dyn.*, 42(11), 1617–1635.
- FEMA. (2000). "State of the art report on systems performance of steel moment frames subject to earthquake ground shaking." *Rep. No. 355c*, SAC Joint Venture for the Federal Emergency Management Agency, Washington, DC.
- Garlock, M., Ricles, J., and Sause, R. (2005). "Experimental studies of full-scale posttensioned steel connections." *J. Struct. Eng.*, 10.1061/(ASCE)0733-9445(2005)131:3(438), 438–448.
- Khoo, H. H., Clifton, G. C., Butterworth, J. W., Mathieson, C. D. (2011). "Development of the self-centering sliding hinge joint." *Proc., 9th*

- Pacific Conf. on Earthquake Engineering Building an Earthquake-Resilient Society*, Auckland, New Zealand.
- Kusumastuti, D. (2005). "A versatile experimentation model for study of structures near collapse: applications to seismic evaluation of irregular structures." Ph.D. dissertation, Dept. of Civil, Structural and Environmental Engineering, Univ. at Buffalo, Buffalo, NY.
- Ma, X., Krawinkler, H., and Deierlein, G. G. (2011). "Seismic design, simulation and shake table testing of self-centering braced frame with controlled rocking and energy dissipating fuses." *Rep. No. 174*, John A. Blume Earthquake Engineering Center, Stanford, CA.
- MacRae, G. A., Clifton, G. C., and Butterworth, J. W. (2009). "Some recent New Zealand research on seismic steel structures." *STESSA09*, Philadelphia.
- Mander, T. J., Rodgers, G. W., Chase, J. G., Mander, J. B., MacRae, G. A., and Dhakal, R. P. (2009). "Damage avoidance design steel beam-column moment connection using high-force-to-volume dissipators." *J. Struct. Eng.*, 10.1061/(ASCE)ST.1943-541X.0000065, 1390–1397.
- Mazzoni, S., McKenna, F., Scott, M. H., and Fenves, G. L. (2009). "Open system for earthquake engineering simulation user command-language manual—OpenSees version 2.0." Pacific Earthquake Engineering Research Center, Univ. of California, Berkeley, CA.
- Papageorgiou, A., Halldorsson, B., and Dong, G. (1999). "Target acceleration spectra compatible time histories." *TARSCHTHS-user's manual*, Engineering Seismology Laboratory, State Univ. of New York, Buffalo, NY.
- Pollino, M., and Bruneau, M. (2008). "Analytical and experimental investigation of a controlled rocking approach for seismic protection of bridge steel truss piers." *Tech. Rep. MCEER-08-0003*, Multidisciplinary Center for Earthquake Engineering Research, State Univ. of New York Buffalo, Buffalo, NY.
- Ricles, J. M., Sause, R., Peng, S., and Lu, L. (2002). "Experimental evaluation of earthquake resistant posttensioned steel connections." *J. Struct. Eng.*, 10.1061/(ASCE)0733-9445(2002)128:7(850), 850–859.
- Rojas, P., Ricles, J. M., and Sause, R. (2005). "Seismic performance of post-tensioned steel moment resisting frames with friction devices." *J. Struct. Eng.*, 10.1061/(ASCE)0733-9445(2005)131:4(529), 529–540.
- Sabelli, R., and Bruneau, M. (2007). "Steel plate shear walls." AISC, Chicago.
- Shishkin, J. J., Driver, R. G., and Grondin, G. Y. (2009). "Analysis of steel plate shear walls using the modified strip model." *J. Struct. Eng.*, 10.1061/(ASCE)ST.1943-541X.0000066, 1357–1366.
- Wang, D. (2007). "Numerical and experimental studies of self-centering post-tensioned steel frames." Ph.D. dissertation, Dept. of Civil and Environmental Engineering, Univ. at Buffalo, Buffalo, NY.
- Webster, D. J. (2013). "The behavior of un-stiffened steel plate shear wall web plates and their impact on the vertical boundary elements." Ph.D. dissertation, Dept. of Civil and Environmental Engineering, Univ. of Washington, Seattle.
- Wiebe, L., Christopoulos, C., Tremblay, R., and Leclerc, M. (2013). "Mechanisms to limit higher mode effects in a controlled rocking steel frame. 2: Large-amplitude shake table testing." *Earthquake Eng. Struct. Dyn.*, 42(7), 1069–1086.
- Winkley, T. B. (2011). "Self-centering steel plate shear walls: Large scale experimental investigation." M.S. thesis, Dept. of Civil and Environmental Engineering, Univ. of Washington, Seattle.